

Tectonic subsidence history and source-rock maturation in the Campos Basin, Brazil

Suzanne E. Beglinger^{1*}, Jan-Diederik van Wees^{2, 3}, Sierd Cloetingh³ and Harry Doust³

¹*Netherlands Research Centre for Integrated Solid Earth Sciences, Department of Tectonics, VU University Amsterdam, de Boelelaan 1085, 1081 HV Amsterdam, The Netherlands*

²*TNO, Business Unit Geo-Energy and Geo-Information, Postbus 80015, 3508 TA Utrecht, The Netherlands*

³*Tectonics Group, Department of Earth Sciences, Faculty of Geosciences, Utrecht University. Postbus 80021, 3508 TA Utrecht, The Netherlands.*

*Corresponding author (e-mail: s.e.beglinger@gmail.com)

ABSTRACT: The Campos Basin is a petroleum-productive, marginal sag basin along the Brazilian margin. It contains a stratigraphic sequence recording lithospheric extension and rift tectonics developing to a fully evolved post-break-up setting. We present a combined approach using subsidence analysis and basin history inversion models to make predictions on source-rock maturation. The classical uniform stretching model does not account for the *observed tectonic subsidence*, and so we consider the thermal and subsidence implications of incorporating different events of magmatic underplating. The post-rift is characterized by one major phase of post-rift thermal subsidence: changes in sediment supply and load, as well as halokinetic movements, cause deviations from normal thermal subsidence and relaxation. The dimensions of these events have been examined and quantified.

Our best-fit forward model is tested against measured borehole temperature (BHT) data. Results show a systematic overestimation of present-day temperatures in the shallow-water wells. Including the effects of hydrothermal convection by raising the conductivity of the top part of the stratigraphic sequence results in an almost perfect fit between predicted and measured BHTs in the shallow-water wells.

Based on these forward models, we predict that the lacustrine shales of the syn-rift Lagoa Feia Fm. could be mature to generate oil and/or gas over a larger area than previously expected. Furthermore, our results suggest that the early post-rift Macaé Fm. is locally mature to generate oil, and that the middle/late post-rift Carapebus/Ubatuba Fm. shales are likely to generate oil as well, if organic-rich facies are indeed present. In light of the most recent pre- and post-salt discoveries made near established oil fields in the Campos Basin, our results support the idea that many more such accumulations may be found.

INTRODUCTION

Marginal sag basins are commonly regarded as quiescent after the transition from rift to drift and during the following subsidence. However, many such basins undergo strata disruption to some degree caused by processes such as halokinesis, post-rift break-up flank uplift or margin instability (Cloetingh *et al.* 2008; Hirsch *et al.* 2010)). The Campos Basin along the Brazilian South Atlantic margin is an example of such a basin. As it contains a stratigraphic record from lithospheric extension and rift tectonics to a fully evolved post-break-up setting, the basin provides an ideal area to study the evolution of a 'passive' continental margin. However, halokinesis forms a major issue in this basin. The effects of halokinesis on subsidence will be discussed as it is responsible for both the creation and destruction of

accommodation space. Similarly, the effect of salt on thermal conductivity and, consequently, on the thermal history will be discussed briefly.

In this study, we will analyse the tectonic subsidence history of the Campos Basin and develop a tectonic model that explains the observed subsidence history. Following Hirsch *et al.* (2010), a combined approach of reverse and forward modelling was applied, in the course of which several model configurations were tested: classical approaches obeying the principles of uniform stretching (McKenzie 1978) were applied and have been expanded further to account for the effects of magmatic underplating. Thermal implications of the obtained models will be analysed and the consequent maturation patterns of different source-rock intervals will be discussed, providing insight into the remaining prospectivity of the basin.

GEOLOGICAL SETTING

The Campos Basin is located on the passive continental margin offshore the state of Rio de Janeiro, SE Brazil (Fig. 1). The basin is about 500 km long and 150 km wide and covers an area of approximately 100 000 km² (at the 3400 m isobath). To the north, the basin is separated from the Espírito Santo Basin by the Vitória High (Vitória–Trindade Chain) and, to the south, it is bounded by the Cabo Frio High, separating it from the Santos Basin.

The tectonic evolution of the Campos Basin is dominated by Mesozoic rifting of the South Atlantic, resulting in the break-up of Pangaea and the development of several basins, whose similarities in tectonostratigraphic evolution point towards a common mechanism of basin formation (Mohriak *et al.* 1990a). The tectonostratigraphic evolution of Campos, and most other basins along the Brazilian margin, can be subdivided into four cycles (Fig. 2) (Cainelli & Mohriak 1999; Guardado *et al.* 2000).

1. *The continental/volcanic pre-rift megasequence*: crustal uplift and the development of peripheral depressions associated with hot spot volcanism, preceding rifting of the continental crust. In peripheral basins, such as Sergipe-Alagoas and Recôncavo-Tucano to the north and Santos Basin to the south, fluvio-lacustrine sediments were deposited (Ojeda 1982).
2. *The continental syn-rift megasequence*: is associated with basement-involved, block-rotated faulting in a rapidly subsiding crust together with widespread mafic volcanism (Mohriak *et al.* 1990a). Neocomian volcanism (135–130 Ma) was a result of the development of the Paraná–Etendeka igneous province (Estrella 1972; Renne *et al.* 1992; 1996; Milner *et al.* 1995; Peate 1997). The sedimentary sequence is composed of lacustrine Barremian deposits (the major proven source rocks known as the Lagoa Feia Fm.) overlying Neocomian basalts. These strata were deposited in a variety of palaeo-environments that were strongly influenced by rift tectonics, such as alluvial fans, fan deltas, carbonate banks and lacustrine environments ranging from fresh to hypersaline.

3. *The transitional megasequence*: represents a phase of tectonic quiescence (Aptian) at the beginning of the drift phase. It contains a lower sequence composed mostly of conglomerates and carbonates and an upper sequence of halite and anhydrite, representing the first seawater inflows from the north (Karner & Gambôa 2007; Scotchman *et al.* 2010).
4. *The marine post-rift megasequence*: can be subdivided into three stages or super-sequences.
 - The first one is made up of Albian shallow-marine carbonates, mudstones and marls (Macaé Fm.) (~ restricted marine post-rift super-sequence). This section is strongly affected by halokinetic movements, causing the development of halokinetic features, such as detached listric normal faults, which sole out on salt (Mohriak *et al.* 1990a).
 - The overlying Upper Cretaceous–Paleocene sequence consists of bathyal shales, marls and sandstone turbidites. This section corresponds to a period of general tectonic quiescence and continuing subsidence (~ open-marine post-rift super-sequence). Residual salt movements still exist and increase in intensity in the deep-water region (Lobo & Ferradaes 1983; Mohriak *et al.* 1990a).
 - The remaining Neogene section is characterized by a progradational sequence of siliciclastics (~ open-marine/deltaic post-rift super-sequence).

As Mohriak *et al.* (1990a) pointed out, several backstripped wells show that the subsidence history of the basin can be attributed to an initial rifting and subsequent thermal recovery of the lithosphere, despite there being some important deviations from the homogeneous simple stretching model (McKenzie 1978). The widespread basaltic magmatism contemporaneous with the rifting is indicative of a thermal anomaly in the mantle (Furlong & Fountain 1986), and the onlapping of Tertiary sediments on the western margin of the basin suggests flexural control on subsidence (Mohriak *et al.* 1987), or distributed, depth-dependent stretching mechanisms (Rowley & Sahagian 1986; Mohriak *et al.* 1990a).

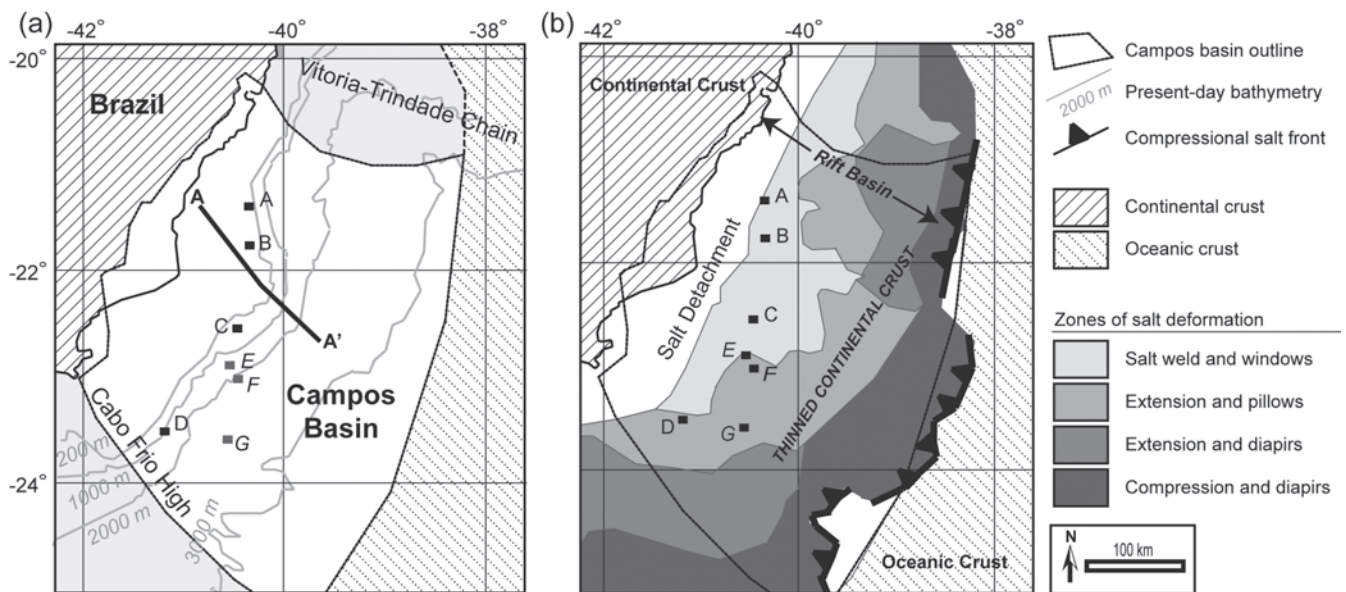


Fig. 1. Campos Basin location maps with well locations (anonymized): (a) present-day bathymetry – section A–A' is shown in Figure 3; (b) main salt structural domains (Meisling *et al.* 2001).

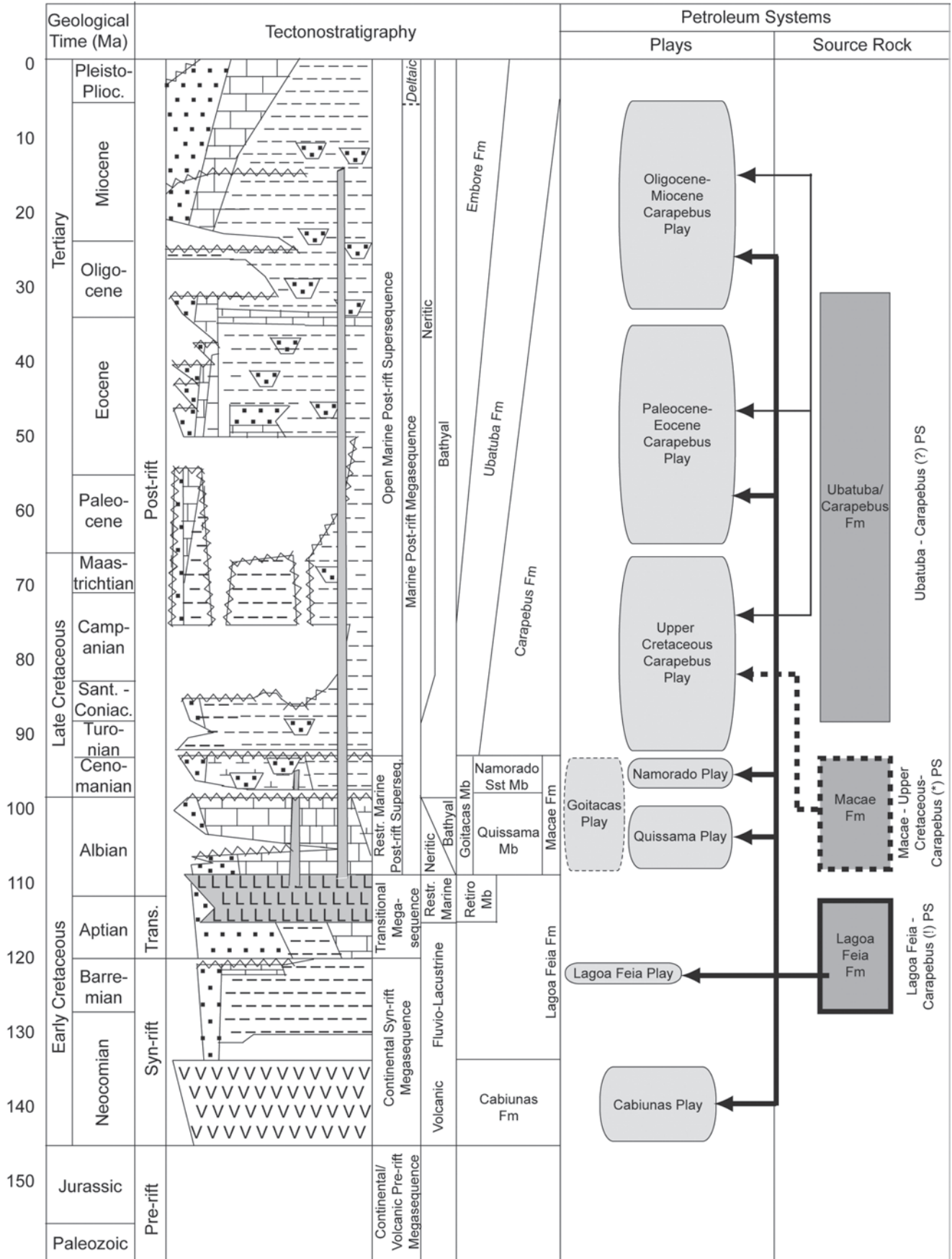


Fig. 2. Tectonostratigraphic chart of the Campos Basin, showing the stratigraphic location of the different elements making up the three petroleum systems (potentially) present in the basin (Mohriak *et al.* 1990a; Chang *et al.* 1992; Cainelli & Mohriak *et al.* 1999; Coward *et al.* 1999; Guardado *et al.* 2000; Meisling *et al.* 2001).

DATA AND METHODS

The database for this study, received from Statoil ASA (Bergen Research Centre, Norway), comprises stratigraphical, lithological and palaeobathymetry data for 7 wells located in the shallow and deep waters of the Campos Basin. Due to confidentiality issues, the wells have been plotted as locations only (Figs 1, 3, 4). Basement is not reached by any of the wells: basement depths were determined from seismic picks in the vicinity of the wells and have an accuracy on the order of ± 50 m. Where given, palaeobathymetry, based on *biostratigraphic* studies in the wells, is indicated by error bars on the subsidence curves (Fig. 5a, b). The tested shallow-water wells are associated with water depths between 0 m and 600 m, and deep-water wells with water depths greater than 600 m.

To gain insights into the interplay of tectonics and subsidence, we follow the same approach as Hirsch *et al.* (2010) in their analysis of the Orange Basin: a combined approach of subsidence analysis and forward modelling (van Wees & Beekman 2000; van Wees *et al.* 2009). A 1D analysis of the well data was conducted in two steps:

- a geohistory analysis was carried out for the wells to determine the tectonic subsidence – the process of deposition was reversed for each well using a backstripping technique;
- 1D forward models for underplating and lithospheric thinning were calculated and compared to the tectonic subsidence derived from backstripping.

Often, tectonic modelling is neglected in the basin modelling workflow and heat flow is generally considered a user input. Our approach, however, allows us to calculate tectonic heat flows, incorporating a variety of tectonic scenarios (van Wees *et al.* 2009). Changes have been successively applied to the forward models until a match between *modelled* and *observed tectonic subsidence* was obtained. These changes relate to different mechanisms that may have influenced the subsidence history, such as uniform or depth-dependent thinning and the effects of underplating (Hirsch *et al.* 2010). Subsequently, maturity has been calculated using tectonic heat flow as input. The predicted present-day temperatures in the wells were measured against actual borehole temperature (BHT) data (internal database Statoil). The modelling methodology is outlined in more detail below.

Backstripping

The aim of backstripping is to analyse the subsidence history of a basin by modelling a progressive reversal of the depositional process (Roberts *et al.* 1998). It is most commonly applied to extensional basins, where it is used to determine the magnitude of lithospheric stretching from post-rift subsidence rates (Sclater & Christie 1980). Stratigraphic units within the sediment column are removed progressively from top downwards. The remaining sediments are decompacted and isostatically restored using Airy isostasy (Hirsch *et al.* 2010). The final restoration accounts for new load conditions, palaeowater depth and the isostatic response to the change in loads. The lithological composition of each well comprises varying fractions of silt, sand, shale, evaporites and carbonates. The reversal of the compaction process follows a double exponential porosity–depth law (Bond & Kominz 1984) (Table 1b). This way, decompaction and its physical impact on density and on thermal conductivity are taken into account as well (Table 1). The quality of any geohistory analysis is fundamentally dependent upon the quality of palaeowater depth information available (Roberts *et al.* 1998), as the water body provides an additional load contribution to the isostatic response of the system and, in turn, to the observed subsidence (Hirsch *et al.* 2010). Generally, palaeowater depths up to 200 m are biostratigraphically well constrained. Uncertainty increases with greater depths.

Backstripping generally produces two subsidence curves.

1. *A basement subsidence curve*, describing the subsidence of the basement as documented in the stratigraphy of the well. This curve consists of two components:
 - the effect of non-tectonic processes such as load-induced subsidence driven by the presence of the overlying sediments and the water body; and
 - the tectonically driven subsidence.
2. *A tectonic subsidence curve* (Fig. 4) solely reflects the tectonic or driving mechanism of a basin, and is obtained by subtracting the load-induced component from the total basement subsidence.

Forward models

We follow a model presented by Van Wees & Beekman (2000) for automatic forward modelling of subsidence data. This approach has been further developed and extended to account

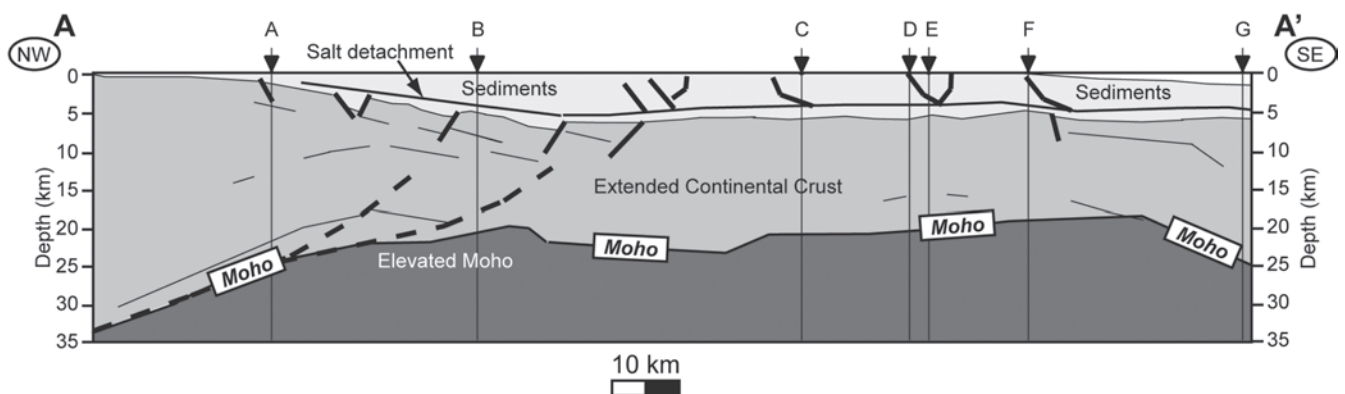


Fig. 3. Geoseismic section A–A' across near-shore shallow Moho anomaly, Campos Basin. NW-dipping master fault is shown to continue downward into the basement, becoming a low-angle extensional detachment at the Moho, with Moho uplift in its footwall (Mohriak & Dewey 1987; Mohriak *et al.* 1990b; Meisling *et al.* 2001 – reprinted by permission of the AAPG whose permission is required for further use). The major detachment surface (within evaporites of transitional cycle) for post-rift salt-induced faults is shown as well. Present-day extended continental crust includes a section of underplated material of varying thickness along strike of the transect. Wells used for modelling in this paper are, in their offset positions, plotted along this line. See Figure 1 for locations of the transect and the wells.

Table 1. Predefined model parameters: (a) thermal parameters in the lithospheric stretching model; (b) parameter table and double-porosity–depth curves used for the decompaction of the sediments throughout the backstripping approach

(a) Model parameters	Units	Value		
Initial lithospheric thickness	km	125		
Initial crustal thickness	km	32		
Surface crustal density	kg m ⁻³	2900		
Surface mantle density	kg m ⁻³	3300		
Surface density underplate	kg m ⁻³	3000		
Crustal conductivity	W °C ⁻¹ m ⁻¹	2.6		
Mantle conductivity	W °C ⁻¹ m ⁻¹	3		
Heat production in the upper crust	10 ⁻⁶ W m ⁻³	0		
Heat production in the lower crust	10 ⁻⁶ W m ⁻³	0.5		
Lithosphere thermal expansion	—	3.5 × 10 ⁻⁵		
Base lithosphere temperature	°C	1330		
(b) Upper part	$\varphi(z) _{z < z_{\text{scale change}}} = \varphi_0 e^{-z/z_{\text{scale}}}$			
Lower part	$\varphi(z) _{z > z_{\text{scale change}}} = \left[\varphi_0 \left(e^{z_{\text{scale change}}/z_{\text{scale}}} / e^{z_{\text{scale change}}/z_{\text{scale} 2}} \right) \right] e^{-z/z_{\text{scale} 2}}$			
	φ_0 (%)	z_{scale} (m)	$z_{\text{scale change}}$ (m)	$z_{\text{scale} 2}$ (m)
Sandstone	35	2300	1000	2000
Shale	68	1500	500	1500
Silt	50	1800	1000	2000
Limestone	50	1400	500	2000
Evaporites	6	7000	20 000	1000

φ is porosity, z is depth (m), φ_0 is surface porosity, $z_{\text{scale change}}$ is depth at which porosity–depth trend changes and z_{scale} and $z_{\text{scale} 2}$ are coefficient rates.

(a) After Mohriak *et al.* (1990b), Chang *et al.* (1992), Aslanian *et al.* (2009), Hirsch *et al.* (2010) and Vilà *et al.* (2010). (b) After Bond & Kominz (1984) and Hirsch *et al.* (2010).

for important effects on heat flow and maturity modelling (van Wees *et al.* 2009). Both pure-shear uniform stretching (McKenzie 1978) as well as depth-dependent differential stretching (e.g. Royden & Keen 1980) can be simulated. Furthermore, the effects of underplating can be determined. The thermal evolution is calculated for the syn-rift evolution and subsequent phases of cooling (van Wees & Stephenson 1995). Here, a minimization technique is used to evaluate those stretching parameters that reproduce the *observed tectonic subsidence* best. Predefined parameters are given in Table 1. A detailed description of the modelling procedure and the physical background is given by van Wees & Beekman (2000) and van Wees *et al.* (2009).

The uniform stretching model predicts the first-order lithospheric response to continental extension (McKenzie 1978; Kusznir *et al.* 1995). Two competing mechanisms occur during rifting: lithospheric thinning is associated with an isostatic response of subsidence, whereas the disturbed lithospheric temperature field and the linked increase in the geothermal gradient cause uplift. The perturbed temperature field re-equilibrates in an exponential manner after rifting ceases. Consequently, the associated subsidence curves show a rapid period of syn-rift subsidence followed by a period of slower time-dependent post-rift subsidence, during which the thermal anomaly, associated with the elevated geotherm from rifting, cools in an exponential manner with a time constant between 60 Ma and 70 Ma (~decay time) (Bott 1992; Kusznir *et al.* 1995; Roberts *et al.* 1998; Hirsch *et al.* 2010)). Departures from the subsidence predicted by the uniform stretching model can be interpreted as additional thermal disturbances to the basin system that are not accounted for (Hirsch *et al.* 2010)). These thermal disturbances may be a result of multi-phase, differential stretching or of magmatic underplating or a superposition of both (Kusznir *et al.* 2005; van Wees *et al.* 2009). The magmatic character of the SE Brazilian continental

margin and the presence of a high density, high velocity body at depth (Mohriak *et al.* 1990b) may indicate that underplating influenced the margin (Gallagher & Hawkesworth 1994).

Heat flow and maturation

A forward model which represents the best-fit tectonic model includes departures from a classical uniform stretching model. However, the models should also be consistent with the presently observed geothermal gradient and basement heat flow, which seem to be relatively low: a geothermal gradient ranging between 18 and 30°C km⁻¹, and averaging around 20°C km⁻¹ (Mohriak *et al.* 1990a) is observed.

Accordingly, we evaluate the thermal history predicted by the forward model and investigate implications for hydrocarbon generation, since the basement heat flow strongly influences the maturity of organic matter throughout basin evolution. The palaeo-thermal gradients are determined through linking tectonic heat flow scenarios and reconstructions of sedimentary conductivity (and heat production) through time. It should be emphasized that in the probabilistic approach, the multiple heat flow scenarios have been deterministically determined as end-members for a sampling of a large range of heat flow scenarios. For model details we refer to Van Wees *et al.* (2009). This modelling approach enables the calculation of maturation based on probabilistic heat flow scenarios, taking into account uncertainties from lithospheric thinning and underplating.

Maturity calculations are based on a time-variable temperature gradient in the basin sediments, in agreement with the calculated tectonic basement heat flow (cf. van Wees *et al.* 2009), and taking into account the effects of depth-dependent porosities in the basin sediments and related changes in thermal conductivity. For the maturity modelling, the Easy%Ro kinetic model of Sweeney & Burnham (1990) was adopted.

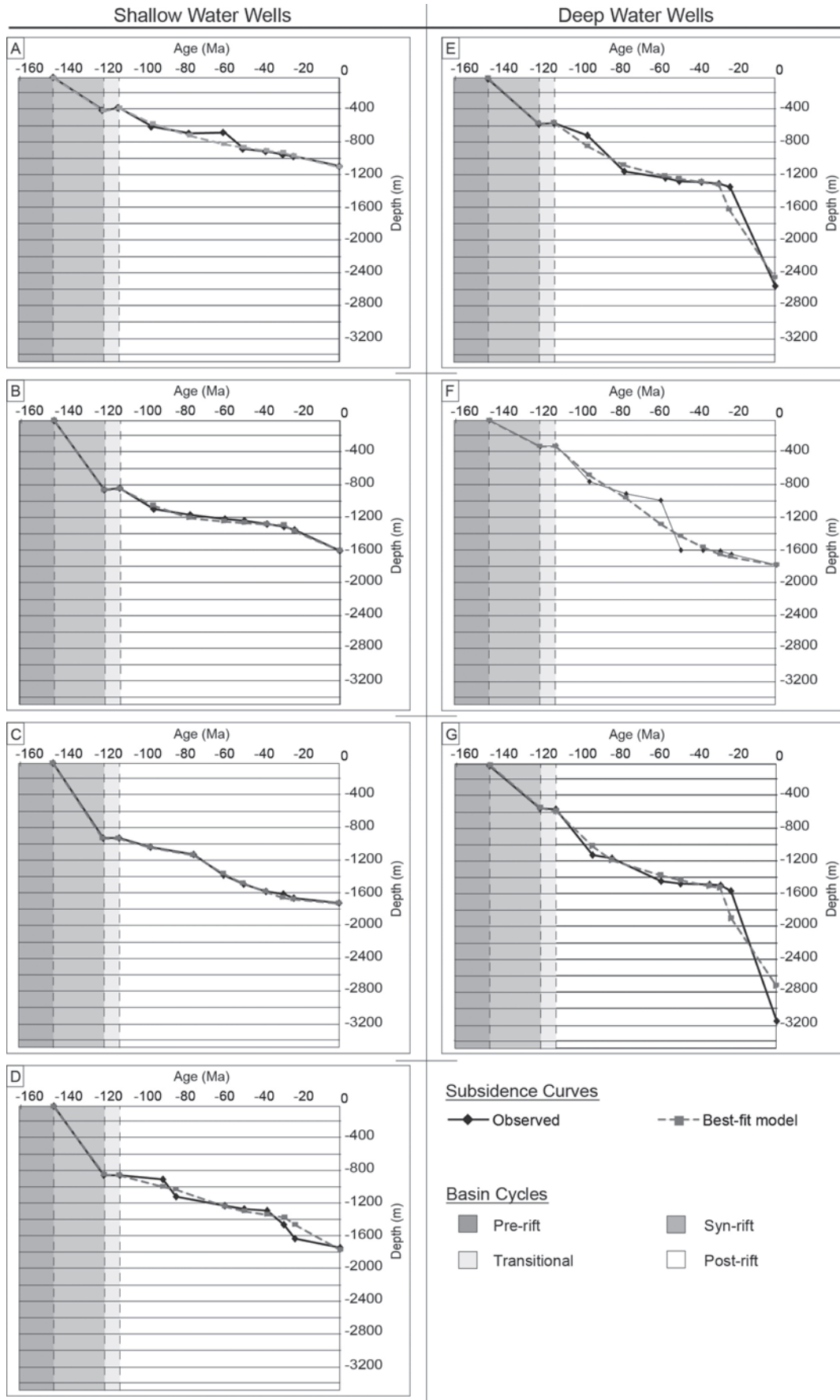


Fig. 4. Tectonic subsidence curves for seven wells (A–G). Solid black lines: *observed tectonic subsidence* (after backstripping). Grey dashed lines: *modelled tectonic subsidence* by best-fit model. See Figure 1 for well locations.

RESULTS

Here, we discuss the different 1D models that we have developed that are consistent with the constraints available from the wells. These constraints include the stratigraphy and lithology-dependent physical properties (Table 1).

Tectonic subsidence

Figure 4 shows the *observed tectonic subsidence* curves after backstripping the sediments penetrated by the wells. Wells are situated both in the shallow- and deep-water domains (Figs 1, 3). During the rifting phase (145.5–120 Ma), all curves are characterized by a moderate to steep slope of initial subsidence. After continental break-up, the transition to the drift phase, the transitional cycle (120–112 Ma), is associated with a decrease in subsidence rates. The curves of the post-rift stage display a common, high-subsidence pulse during Albian times, compatible with the thermal cooling of attenuated continental lithosphere. The post-rift phase shows some variations in subsidence pattern for each well, but a general first-order trend of ‘normal’ thermal cooling can be recognized.

Forward models

Pure shear versus syn-rift underplating models. After obtaining the tectonic subsidence history of the wells from backstripping, we tried to find forward models that reproduce this *observed subsidence pattern*. All tested models involve an initial lithospheric thickness of 125 km (Chang *et al.* 1988; 1992; Karner & Gambôa 2007) and a crustal thickness of 32 km (Chang *et al.* 1992; Karner & Gambôa 2007; Aslanian *et al.* 2009). The model that best fits the *observed tectonic subsidence* is plotted for all wells in Figure 4. The models obtained for shallow-water well A and deep-water well E (Fig. 5) are shown to illustrate the differences between the tested forward models (and which are representative for all other wells). For reference, Figure 5 also shows, as additional information, the range of palaeowater depths through time for both wells.

The first model tested in order to fit the *observed tectonic subsidence* (Fig. 5c, d) concerns the uniform stretching model (McKenzie 1978). The instantaneous stretching factor β for both crust and mantle associated with wells A and E (obtained by fitting a McKenzie curve to the backstripped subsidence curves) is 1.28 and 1.53, respectively (Fig. 5e). These stretching factors are responsible for the creation of an initial basin depth of 516 m and 794 m, respectively (Fig. 5c–e). The model also predicts thicknesses of the present-day crystalline crust of 25 km and 20.9 km, respectively (Fig. 5e), which is systematically too thick compared to the present-day thickness as derived from deep seismic data (Fig. 3, 5e) (Mohriak & Dewey 1987; Mohriak *et al.* 1990b; Meisling *et al.* 2001). However, an intensification of stretching, particularly in the deep-water region, would further deepen the initial basin, which is already far too deep when compared to the initial basin depths of 408 m (well A) and 561 m (well E) in the backstripped curves (Fig. 5c–e).

Subsequent to rifting, thermal cooling commenced causing uniform continuous subsidence of a basin steadily increasing in depth. However, the modelled present-day basement depth is too shallow compared with the *observed depth*, particularly in the deep-water well (Fig. 5c, d). Also, neither variation of β nor of the initial lithospheric thickness results in a good approximation to the *observed tectonic subsidence*, as the initial subsidence is always too fast. Finally, later phases of increasing or decreasing subsidence rates are unaccounted for by the standard McKenzie model. Therefore, a number of effects have been included in the forward models, which deviate from the uniform stretching model.

An important consequence of lithospheric thinning (Fig. 6a, b) is the change in pressure that occurs adiabatically, resulting in partial melting of harzburgites and other mantle rocks. As these melts migrate upwards, they can mix with crustal rocks and either extrude or become trapped into the lower crust as massive underplated bodies (Cox 1980; Furlong & Fountain 1986; Mohriak *et al.* 1990b). Here, we consider the effect of underplating, which is cumulatively emplaced during the syn-rift phase in our forward models. Note that the modelling procedure used assumes that the cumulatively emplaced, underplated body is not affected by stretching. This might be regarded as an oversimplification, but allows for a first-order understanding of the effects of underplating. The underplated body becomes part of the crystalline crust within the post-rift phase (Hirsch *et al.* 2010). Rifting was superposed on to and during the emplacement of the Serra Geral tholeiites, which were subaerially extruded across a large part of the area. These voluminous tholeiitic basalts are diagnostic of significant partial melting of asthenospheric material at elevated temperatures, which might be a result of plume activity (Karner 2000). The amounts of melt generated are dependent on extension velocity and mantle temperature (van Wijk *et al.* 2001). Modelling performed by Mohriak *et al.* (1990b) suggests that the ideal density model would require variable densities in the crust with a lower density differential between the crust and mantle near the apex of the mantle upwarping; this might be a reasonable possibility if there is underplating. We have defined the density of the underplated material to be 3000 kg m⁻³ and assume an emplacement temperature of 1300°C. If these melts get trapped underneath the crust, they replace denser lithospheric mantle; when isostasy applies, this will result in uplift compared to a uniform stretching model without magmatic activity.

We assume that the lower crustal, high density body pointed out by Mohriak *et al.* (1990b) represents a certain volume of underplated magma. Gallagher & Hawkesworth (1994) proposed that the present-day average elevation of the onshore margin is attributable entirely to underplating and, therefore, estimated an underplated thickness of between 3.3 km and 4.2 km (Gallagher & Hawkesworth 1994). Initially, we incorporate 4.2 km of underplating in our forward models. For wells A and E, this underplating causes a decrease in the initial basin depth to 385 m and 661 m, respectively (Fig. 5c–e). In the case of shallow-water well A, the consideration of 4.2 km of underplated material results in a good match with the backstripped tectonic subsidence. However, for deep-water well E more underplating seems required to better approximate initial subsidence. Associated β factors increase to 1.47 and 1.82, respectively, resulting in a predicted present-day crustal thicknesses of 21.8 km and 17.6 km, respectively (Fig. 5e). However, the predicted crustal thickness for the shallow-water well is now too thin, while that for the deep-water well is still too thick (Figs 3, 5e). To obtain the correct thicknesses (with an error range of 10%), we need to make further changes to the underplating thickness and β factors.

As a consequence of underplating, the thermal regime of the early stages of basin evolution is affected, since the addition of hot material causes a significant rise in basement heat flow (Fjeldskaar *et al.* 2003; Allen & Allen 2006). Heat flow evolution is compared for both the pure shear and ‘4.2 km syn-rift underplate’ models (Fig. 6c, d). In the case of the uniform stretching model, rifting is accompanied by an increase in basement heat flow by ~ 2 or 4 mW m⁻² (Fig. 6c, d). Incorporating syn-rift underplating elevates the peak heat flow by *c.* 10 mW m⁻² for the syn-rift phase (Fig. 6c, d). However, underplating not only influences the initial stages of basin evolution, but also affects the post-rift subsidence pattern. Because of the addition of hot material, the post-rift thermal cooling becomes more effective (Dupré

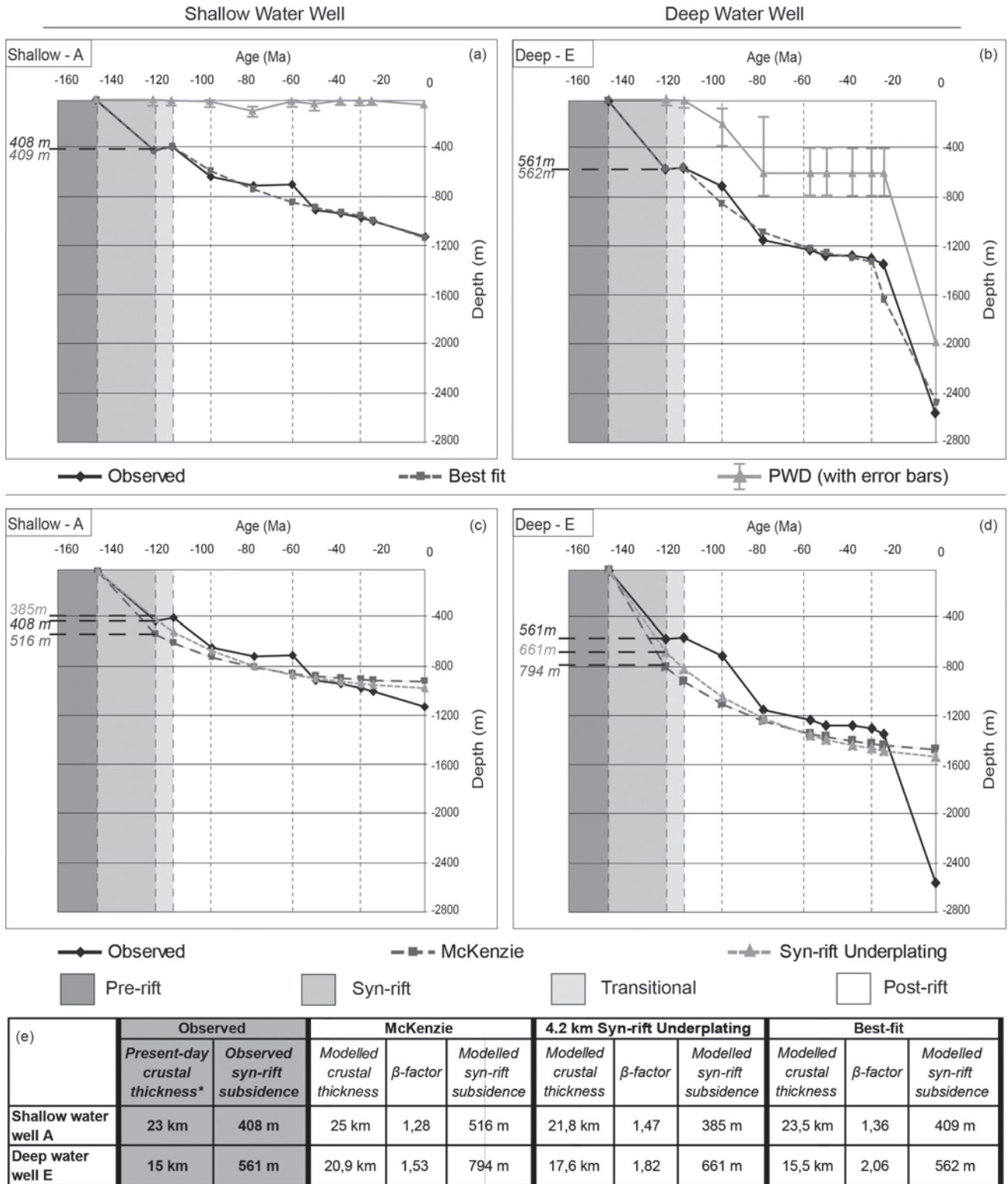


Fig. 5. Observed and modelled tectonic subsidence curves for shallow-water well A and deep-water well E. (a) Shallow-water well A – observed tectonic subsidence after backstripping versus modelled tectonic subsidence according to the best-fit forward model. (b) Deep-water well E – observed tectonic subsidence after backstripping versus modelled tectonic subsidence according to the best-fit forward model. Both (a) and (b) include the palaeowater depth evolution (with error bars) for the wells as used in the modelling (internal database Statoil). (c) Shallow-water well A – observed tectonic subsidence after backstripping versus modelled tectonic subsidence according to the uniform stretching (McKenzie 1978) and 4.2 km syn-rift underplating forward models. (d) Deep-water well E – observed tectonic subsidence versus modelled tectonic subsidence according to the uniform stretching (McKenzie 1978) and 4.2 km syn-rift underplating forward models. (e) Summary of present-day crustal thickness (including a varying thickness of underplated material) (Mohriak & Dewey 1987; Mohriak et al. 1990b; Meisling et al. 2001) in the two wells, as well as the observed syn-rift subsidence (after backstripping), plus the results of the three forward models. Depth values along the vertical axes of (a)–(d) correspond to initial syn-rift subsidence as derived from backstripping and as predicted by each forward model (text colour indicates associated model). β factors represent effective thinning factors.

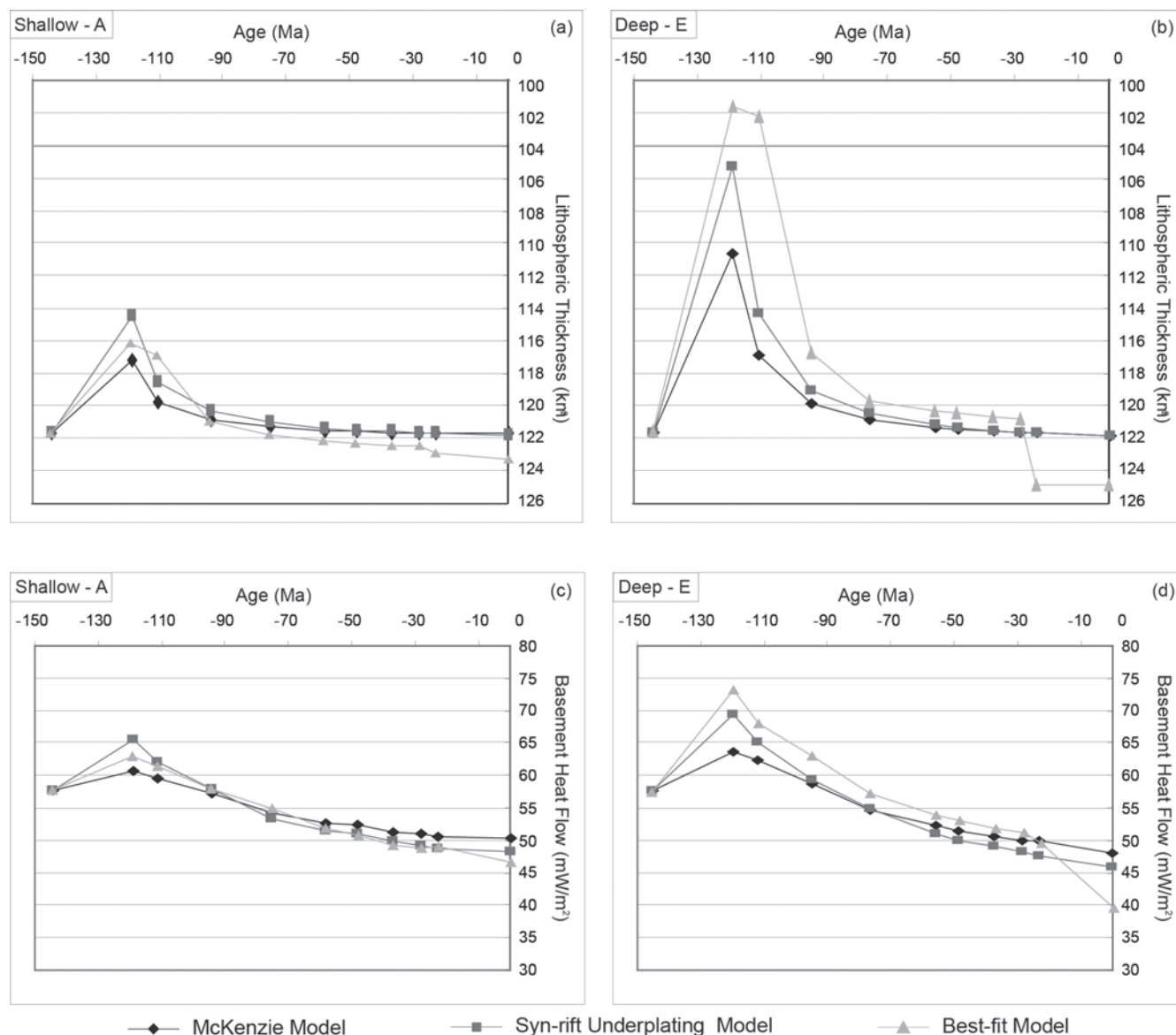


Fig. 6. (a, b) Development of lithospheric thickness for shallow-water well A and deep-water well E, respectively, as predicted by the three forward models. (c, d) Heat flow evolution for shallow-water well A and deep-water well E, respectively, as predicted by the three forward models.

et al. 2007) and the final basement depth is predicted to be deeper than in the case of the McKenzie model (Fig. 5c, d).

We have seen that implementing underplating in the early stages of basin evolution improves the fit between observations and forward models. However, the model does not account for the observed phase of uplift during the transitional cycle or the changing subsidence rates during the post-rift. These phases are documented for many passive margins and the related mechanisms are still a matter of debate (Watts & Fairhead 1999; Fjeldskaar *et al.* 2003; Gernigon *et al.* 2004). Possible causes behind margin uplift include phases of sub-crustal thinning, rift shoulder uplift in consequence of renewed extension, far-field compression due to ridge-push forces (Cloetingh *et al.* 2008) or additional thinning of the sub-crustal mantle in response to either mantle plumes or small-scale convection (Boutillier & Keen 1999).

2-phase underplating model. In the previous sections we identified a number of challenges which need to be addressed by alternative model scenarios to construct a valid model.

1. Present-day crustal thickness predicted by the standard McKenzie model overestimates the thickness compared to the actual present-day values (Figs 3, 5e). This suggests that we need to increase the McKenzie crustal stretching factor β of 1.28 and 1.53 for the shallow- and deep-water wells, respectively (Figs 3, 5e). However, increasing β will cause greater syn-rift subsidence, incompatible with the subsidence observations (Figs 3, 5e). The elevated position of the (rift) system (at least until break-up) has also been observed in other South Atlantic marginal basins (Dupré 2003; Moulin *et al.* 2005; Aslanian *et al.* 2009).
2. To allow for more crustal stretching, we need a mechanism, such as underplating, to counteract subsidence by uplift (Skogseid *et al.* 2000). Adopting a syn-rift underplate of 4.2 km thick for both the shallow and deep wells results in increased β factors of 1.47 and 1.82, respectively (Figs 3, 5e). The predicted present-day crustal thickness is now thinner than observed in shallow-water well A, but still thicker than observed in deep-water well E (Figs. 3, 5e).

Table 2. Results of the best-fit forward model for all wells, including syn-rift crustal (effective) stretching factors (β), consequent modelled present-day crustal thicknesses (including underplated material) and required thicknesses of underplated material

Events		Syn-rift (145.5–120.0 Ma)		Transitional (120.0–112.0 Ma)	Modelled present-day crustal thickness (km)
		β	Underplate thickness (m)	Underplate thickness (m)	
Shallow water	A	1.36	2500	400	23.5
	B	1.87	2500	400	17.1
	C	2.01	2500	10	15.9
	D	2.26	4700	200	14.2
Deep water	E	2.06	7000	200	15.5
	F	2.08	10 000	200	15.4
	G	1.75	5500	200	18.3

- The model results suggest that a homogeneous distribution of the underplate thickness is incompatible with the observed crustal thickness. Scenarios with variations in underplate thickness were tested and a best-fit model is presented in Table 2.
- During the transition from rift to full drift conditions (the transitional cycle), the wells show a decrease or stagnation in tectonic subsidence (Figs 4, 5), which does not match predictions of thermal subsidence in the McKenzie model, in which thermal subsidence rates are highest immediately after rifting, and decrease gradually afterwards. The presence of evaporites in the transitional cycle overlain by post-rift carbonates (Aslanian *et al.* 2009) seems to indicate that this elevated position was maintained until well within the early post-rift. To explain the temporary stagnation in subsidence (rate), we require a mechanism for temporary uplift. Crustal thinning cannot explain this, since no crustal extension takes place post-break-up. This leaves open two other options to explain the elevated position: strong mantle thinning or continued underplating. We assume that mantle thinning is a regional process. However, to fit the observed subsidence during the transitional cycle some wells require mantle thinning ($\delta > 1$; wells A, B, E and F), while others require mantle thickening ($\delta < 1$; wells C, D and G) during this cycle. Also the distribution of the wells mixes up these δ values, so no trend can be distinguished. However, since underplating was already an active process during rifting and should normally be most active during break-up times, we adopted additional underplating during the transitional cycle with varying thicknesses of underplated material between 10 and 400 m (Table 2).
- During the post-rift, starting at 112 Ma, when proper drift conditions are met, we observe several variations in the subsidence patterns of the different wells. However, the best-fit model for all wells together describes one phase of normal thermal subsidence and relaxation, allowing the lithosphere to regain its thickness (Table 2) and no distinct phase of additional subsidence associated with crustal thinning, no phases of uplift, associated with potential additional underplating or sub-crustal thinning (Hirsch *et al.* 2010).

The best-fit model for the shallow-water well results in a β factor between those predicted by the other two forward models (Fig. 5a, e; Table 2). Similarly, the final lithospheric thickness as well as the increase in heat flow, due to rifting (at 120 Ma), are of an intermediate value (Fig. 6a, c).

In the deep-water well, much more syn-rift crustal extension is required to obtain the present-day crustal thickness. To

compensate for the associated increase in subsidence, the emplacement of a much thicker underplate is required than the initial 4.2 km (Fig. 5b, e; Table 2). Consequently, lithospheric thinning due to rifting is much stronger (Fig. 6b), and the same applies to the increase in heat flow (Fig. 6d).

The incorporation of underplating during the transitional cycle, although thin, causes the lithosphere to regain its thickness more slowly than the other models predict (Fig. 6a, b). Also, the basement heat flow seems to decrease less rapidly (Fig. 6c, d).

Finally, due to addition of (more) hot material, the post-rift thermal cooling also becomes more effective and the final basement depth is deeper than predicted by the other models (Fig. 5a, b).

Thermal convection

The best-fit tectonic model has been tested against BHT data (internal database Statoil). Figures 7e–g demonstrate that the predicted present-day temperatures within deep-water wells E, F and G agree with the measured BHTs. However, in shallow-water wells B, C and D, the predicted temperatures are systematically 20–30°C higher than the measured BHTs (Fig. 7b–d). This difference in temperatures can be explained by an additional process of hydrothermal convection active within the upper part of the stratigraphic section in the shallow parts of the basin. Hydrothermal convection leads to an increase in conductivity, resulting in more effective cooling of the basin sediments (e.g. Luijendijk *et al.* 2011). Consequently, the influence of moving water is an important factor in shaping temperature–depth curves (Renner *et al.* 1975; Rannali & Rybach 2005).

Although we cannot model for actual hydrothermal convection, we can model for the increase in conductivity in the top section of the sediments, which is most likely affected strongest by thermal convection (Luijendijk *et al.* 2011) and can be used as a proxy in a conductive model (Spinelli & Fisher 2004). Increasing the conductivity 2–4 times with respect to the original conductivity of the stratigraphic section covering the last 23 Ma (mixed shales, sandstones and limestones), a significant decrease in temperature is established fitting the measured BHT data (Fig. 7b–d).

Shallow-water well A is much different compared to wells B, C and D as the predicted present-day temperatures are actually 20–30°C lower than the measured BHTs, rather than higher. Considering our modelling results, this implies either an overestimation of the sediment conductivity in this well (unlikely) or the nearby presence of advective heat (e.g. a channel of fault-related upward-moving fluids). We consider it beyond the scope of this study to find an explanation for this anomaly.

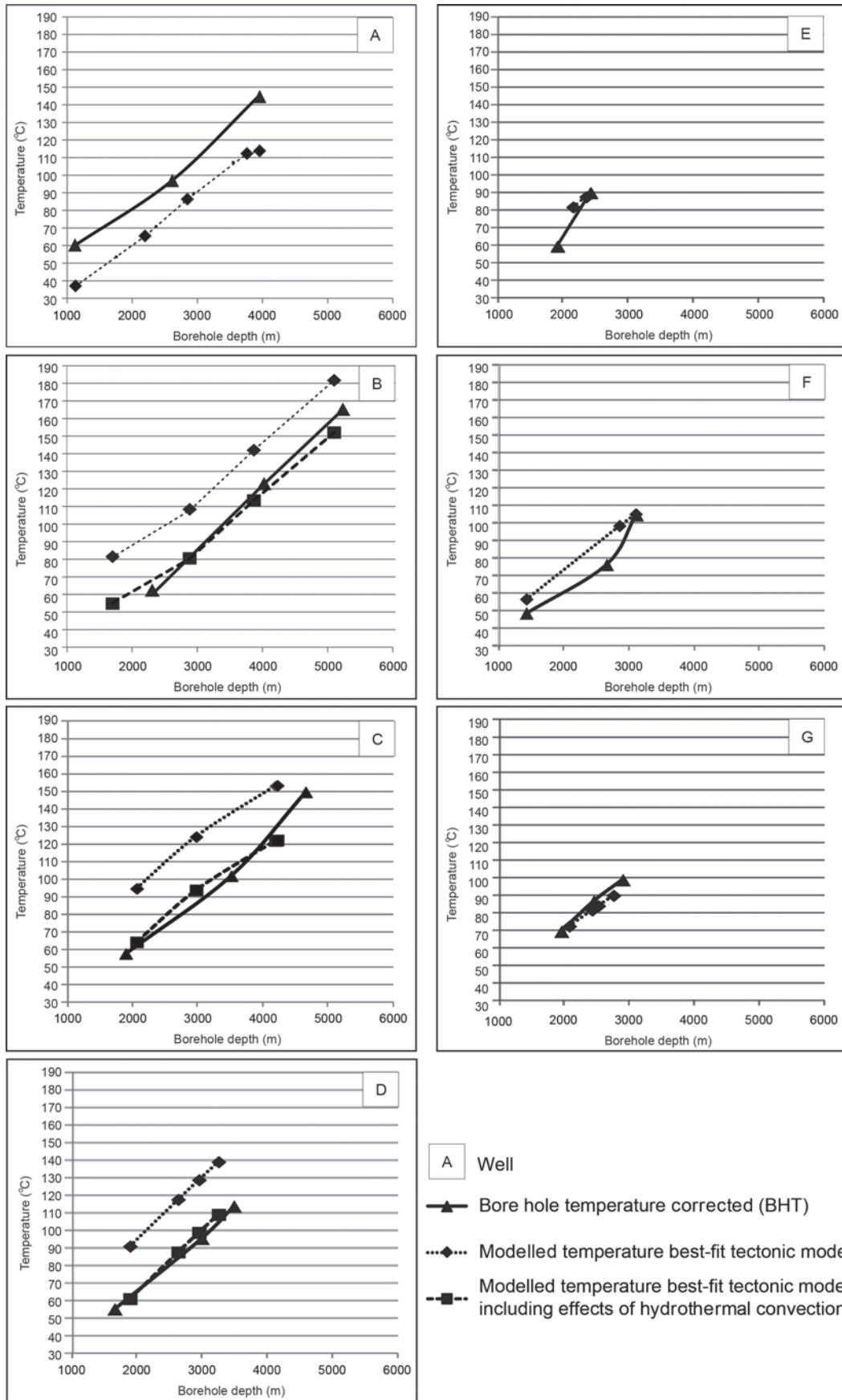


Fig. 7. Predicted present-day well temperatures versus measured borehole temperature data (internal database Statoil). Note that before including the effect of hydrothermal convection, the predicted present-day well temperatures in shallow-water wells B, C and D were systematically too high (20–30°C). Hydrothermal convection seems inactive in deeper parts of the basin. Shallow-water well A is the only well showing a 20–30°C underestimation of the well temperatures.

DISCUSSION

Basin cycle evolution

Syn-rift cycle. The Moho became uplifted during Early Cretaceous rifting and crustal extension. The dominant vergence of the extensional faults is landward, and Meisling *et al.* (2001) infer that the SW-dipping master fault continues downward into the basement, becoming a low-angle extensional detachment at the Moho, with the Moho uplifted in its footwall (Fig. 3). This detachment is suggested originally to have been a Brasiliano (Pan-African) thrust fault, which became reactivated during Neocomian rifting: the vergence of the Neocomian rifts is inherited from the vergence of the Brasiliano fold belts (Mohriak & Dewey 1987; Mohriak *et al.* 1990b; Meisling *et al.* 2001).

Generally, uniform stretching results in an increasing tectonic subsidence from the proximal to distal domains of a basin (e.g. Hirsch *et al.* 2010)). Mohriak *et al.* (1990b) pointed out that backstripped wells in the Campos Basin indicate an increase in stretching factor from values slightly greater than 1.0 in the western region to values slightly smaller than 2.0 towards its depocentre. However, our shallow-water wells show a greater syn-rift subsidence than the deep-water wells (except well A). Using crustal thinning factors as our constraints, we need increasing basinward thicknesses of underplating to explain the elevated position of the rift basin in the deep-water region.

Gallagher & Hawkesworth (1994) argue that, considering the regional elevation of the basin relative to present-day sea-level, an underplate thickness between 3.3 km and 4.2 km is required. Our results for underplate thickness in the shallow-water region agree with this statement (Table 2). However, moving further offshore (already starting at 'shallow water' well D), more underplating is required to explain the initial, relatively shallow, syn-rift tectonic subsidence and the present-day crustal thickness: a maximum underplate thickness of 10 km is modelled at deep-water well F (Table 2). Our results for underplating agree with those of Hirsch *et al.* (2010), who calculated a thickness of the underplated material between 3 km and 14 km across the Orange Basin.

Note that:

- our maximum β factor reaches a value of 2.26 in well D (Table 2) located in the main depocentre, exceeding the proposed 2.0 by Mohriak *et al.* (1990b);
- the region of the most distal well G is characterized by a greater crustal thickness and, therefore, smaller β factor, than wells C, D, E and F (Table 2);
- the required syn-rift underplating in the most distal part of the basin (near well G), decreases significantly compared to areas near wells D, E and F (Table 2).

At the same time, the lithosphere experiences a thinning to less than 116 km in the domain closest to the shore (Fig. 8a) and to less than 96 km in the main depocentre during rifting (Fig. 8a). Further offshore, lithospheric thinning seems to decrease again (Fig. 8b): this may be explained by thermal doming of hot mantle material underneath the main depocentre of the basin (Fig. 3). This might also explain the initial thinning followed by thickening of the crust moving further offshore (and hence the increasing and decreasing β factors) and, similarly, the changes in syn-rift underplate thickness from the nearshore to the distal domain (Table 2).

However, Foucher *et al.* (1982) demonstrate that a greater degree of lithospheric thinning is required to produce any melts, even by instantaneous rifting, than we have modelled here. Furthermore, Pedersen & Ro (1992) demonstrate that a stretching factor of 4 is needed to make a solidus cross-over, if the

thinning occurs over a 10–20 Ma time period. Consequently, a thermal anomaly in the mantle, i.e. mantle plume, which is not isostatically compensated, is required to explain our results. The intense magmatic activity during the Early Cretaceous syn-rift cycle is considered to have been a consequence of the Tristan da Cunha mantle plume (Hawkesworth *et al.* 1992; Mizusaki *et al.* 1992; Wilson 1992; Thompson *et al.* 1998; An & Assumpção 2006; Fetter *et al.* 2009): the extruded (syn-rift) basalts have a similar geochemical signature to that of the continental flood basalts of the Paraná Basin magmatic province (Karner 2000; Fetter *et al.* 2009). To produce these voluminous basalt flows, extensive partial melting in the upper mantle is required and would probably be accompanied by magmatic underplating (An & Assumpção 2006) in the area in and around the Campos Basin.

It might be argued that our modelled underplate thickness (reaching a maximum thickness of 10 km) indicates a percentage of partial melting that is significantly higher than that involved in the process of seafloor spreading of the South Atlantic, responsible for the creation of only *c.* 6 km of igneous rock. This may be an artefact of our modelling procedure, which relies entirely on the concept of kinematic stretching. On the other hand, Ziegler (1992) points out that stress-induced extension of the lithosphere, resulting in decompression of its lower parts and of the upper asthenosphere, is likely to cause a greater degree of partial melting in areas underlain by abnormally hot asthenospheric (e.g. affected by mantle plumes, as in the Campos Basin) than in areas underlain by normal temperature mantle. Consequently, less lithospheric thinning is required to produce similar volumes of melts.

Note that our modelling procedure allows for only kinematic stretching and cannot account for variable asthenospheric temperatures and/or lithosphere thickness. Further research on the deep crustal structure of the Campos Basin, as well as more extensive thermal modelling with respect to the thermal anomaly, underplating and consequent basin subsidence and heat flow evolution is highly recommended.

Transitional cycle. Normally, subsequent to rifting and the emplacement of underplating, thermal cooling starts and causes the system to re-equilibrate to regain the thickness of the previously stretched lithospheric mantle. However, the subsidence curves of the backstripped wells show a stagnation or even decrease in subsidence rate from 120 Ma to 112 Ma (Figs 4, 5), in contrast to the strongly increased subsidence during this phase in the Orange Basin, which seems to be dominantly tectonically induced (Hirsch *et al.* 2010). Since no crustal extension is continuing, and sub-crustal thinning is not able to explain this subsidence pattern, we need to incorporate an extra phase of underplating. The additional thickness of the modelled underplated material decreases from 400 m in the nearshore domain to 0–10 m in the main depocentre and increases again to about 200 m in the most distal domain (Table 2). As a consequence of this additional underplating, the thinned lithosphere regains its original thickness more slowly (Figs 6a, b, 7) and, similarly, the associated heat flow remains elevated as well (Fig. 6c, d).

Post-rift cycle. From 112 Ma onwards, smooth tectonic subsidence curves of moderate gradients indicate that a tranquil phase of thermal subsidence prevailed in the basin until the present day. Our best-fit model does not show any signs of sub-crustal thinning during the post-rift phase, in contrast to the two post-rift sub-crustal thinning phases demonstrated by Hirsch *et al.* (2010) in the Orange Basin (74–67 Ma and 16–14 Ma). However, since 112 Ma, sedimentation rates decreased until a minimum was reached during the Late Cretaceous first-order

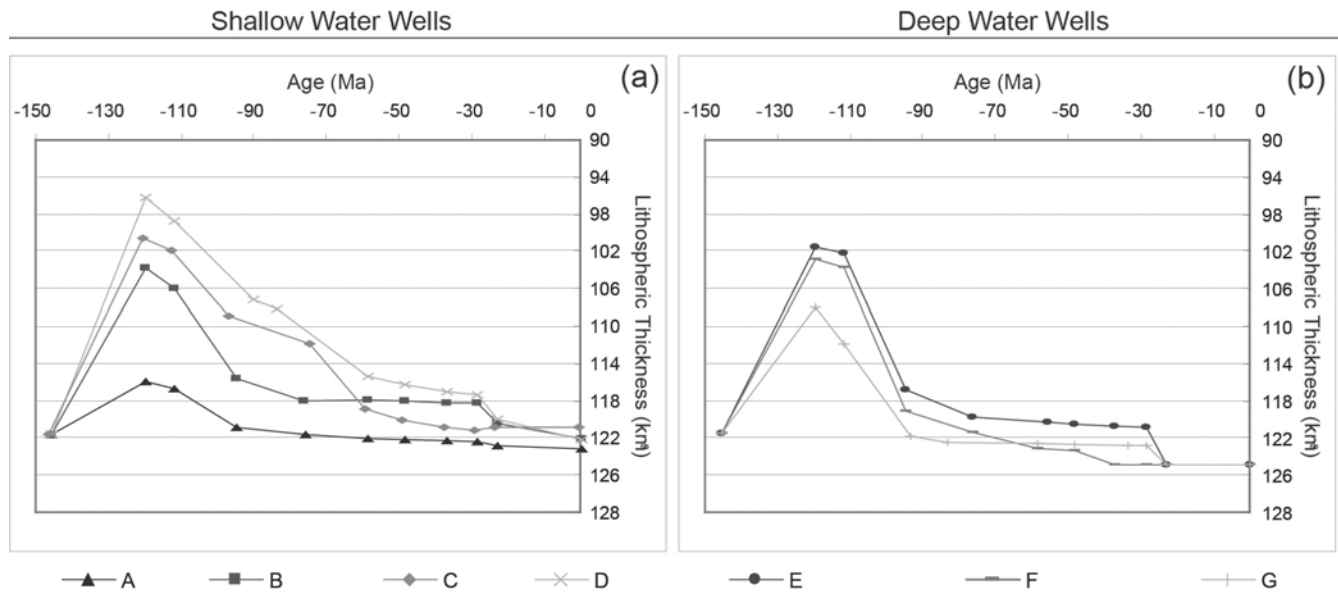


Fig. 8. Lithospheric thickness evolution through time as predicted by the best-fit forward model: (a) shallow-water wells; (b) deep-water wells.

Table 3. Properties of known (drilled) potential source-rock intervals in the Campos Basin

Source-rock properties		
Basin cycle	Formation name	Properties
Post-rift (112–0 Ma)	Carapebus/Ubatuba Fm. (± 90 –0 Ma)	Deep-marine shales and calcareous mudstones Low TOC Low HI Low S ₂ Reflecting highly oxygenated conditions
	Macaé Fm. (112– ± 90 Ma)	Anoxic deep-marine shales Type II kerogen Moderate TOC ~ Equivalent to Urucutuca Fm. shales in Espírito Santo Shallow-marine shelf marls Type III kerogen Max. TOC: 1% Reflecting shallow oxygenated marine shelf environment
		Deeper-marine marls Type II kerogen Max. TOC: 3% ~ Equivalent to Regencia Fm. in Espírito Santo
Transitional (120–112 Ma)	*	*
Syn-rift (145.5–120 Ma)	Lagoa Feia Fm. (130–120/112 Ma)	Well-laminated lacustrine shales interbedded with carbonates Type I kerogen Fresh, brackish to saline waters Avg. TOC: 2–6% Max. TOC: 9% Max. HI: 900 mgHC mg ⁻¹ TOC Max. S ₂ : 38 mgHC g ⁻¹ rock Avg. API gravity: 17–37° API
Pre-rift (>145.5 Ma)	*	*

After Mohriak *et al.* (1990a), Mello *et al.* (1994), Coward *et al.* (1999), Guardado *et al.* (2000) and Khain & Polyakova (2004). *no information available

highstand in eustatic sea-level (Chang *et al.* 1992), resulting in transgressive sedimentary patterns (Contreras *et al.* 2010). The end of this period of basin starvation is essentially controlled by a lack of sediment supply driven by local tectonics (Chang *et al.* 1988; 1992). This period was followed by a phase of higher subsidence rates during the Tertiary, which was mainly the effect

of sedimentary loading of the lithosphere in response to high clastic supply, resulting in rapid shallowing of the basin and seaward progradation of the shelf (Chang *et al.* 1992). During Late Cretaceous/Early Tertiary times, uplift of the Serra do Mar mountain range caused a shift in the original drainage patterns from the Santos towards the Campos Basin (Modica & Brush

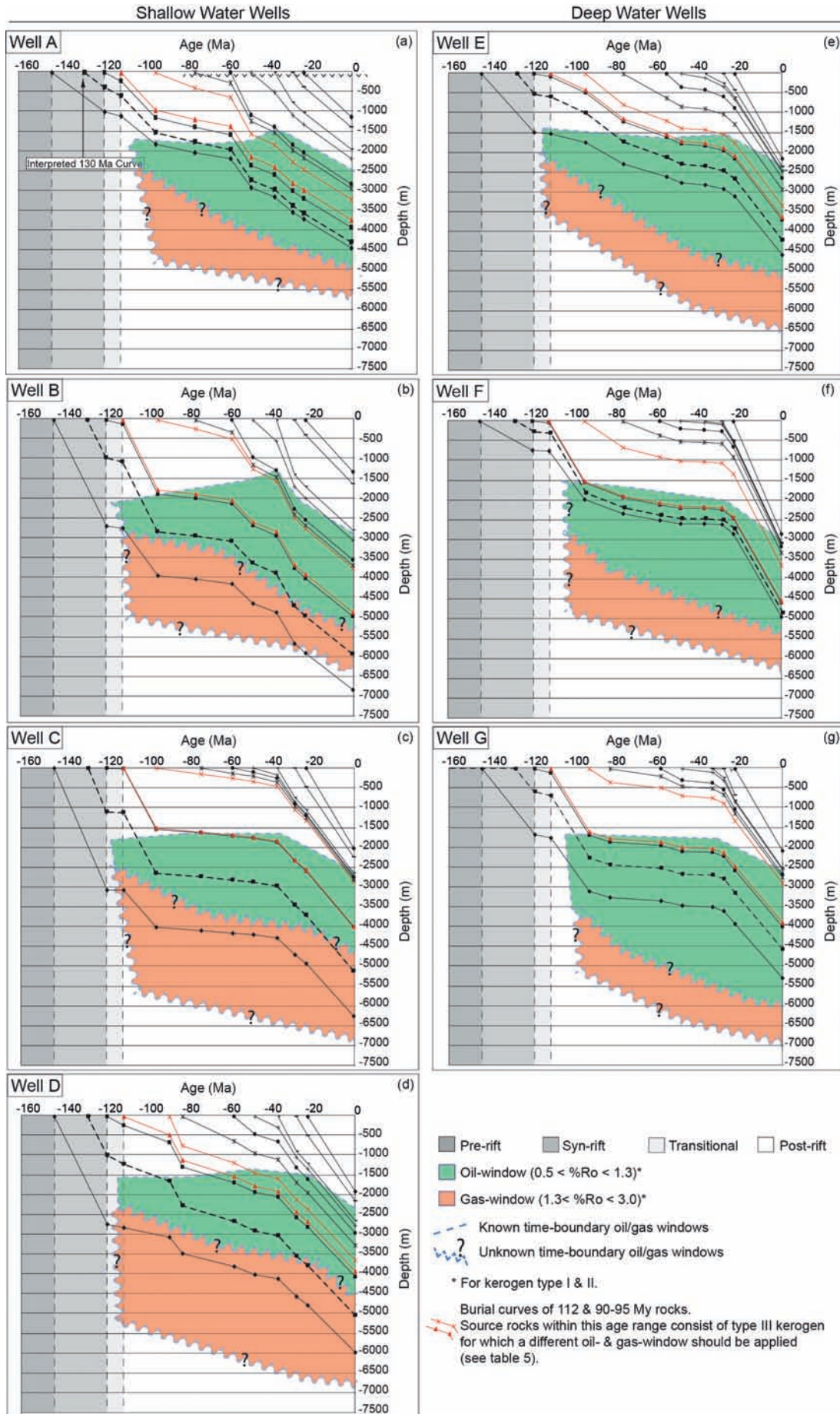


Table 4. Summary of (range of) timing of oil and gas generation for two (potential) source-rock intervals in all wells: the Lagoa Feia Fm. (145.5–112 Ma) and the Carapebus Fm. (90–0 Ma)

Wells	Source formation	Top/bottom ages (Ma)	Time entering oil window (Ma)	Time entering gas window (Ma)	Time entering: overmature (Ma)	Present-day window
A	Lagoa Feia	145.5	112–95	—	—	*
		112	58.7–48.6	—	—	*
	Carapebus	95	48.6–37.2	—	—	*
		<u>58.7</u>	37.2–28.45	—	—	*
		0	—	—	—	
B	Lagoa Feia	145.5	120–112	112–95	23.03	***
		112	95–76.4	23.03–0	—	**
	Carapebus	95	48.6–37.2	—	—	*
		<u>37.2</u>	23.03–0	—	—	*
		0	—	—	—	
C	Lagoa Feia	145.5	?	120–112	—	**
		112	74–58.7	—	—	*
	Carapebus	95	23.03–0	—	—	*
		<u>28.45</u>	23.03–0	—	—	*
		0	—	—	—	
D	Lagoa Feia	145.5	?	120–112	23.03–0	***
		112	83.5–58.7	—	—	*
	Carapebus	95	58.7–48.6	—	—	*
		<u>28.45</u>	23.03–0	—	—	*
		0	—	—	—	
E	Lagoa Feia	145.5	120–112	—	—	*
		112	55.8–48.6	—	—	*
	Carapebus	95	37.2–28.45	—	—	*
		<u>37.2</u>	23.03–0	—	—	*
		0	—	—	—	
F	Lagoa Feia	145.5	112–95	—	—	*
		112	95–76.4	—	—	*
	Carapebus	95	23.03–0	—	—	*
		<u>28.45</u>	23.03–0	—	—	*
		0	—	—	—	
G	Lagoa Feia	145.5	112–93.5	—	—	*
		112	83.5–58.7	—	—	*
	Carapebus	95	23.03–0	—	—	*
		<u>58.7</u>	23.03–0	—	—	*
		0	—	—	—	

The underlined age given in each well for the Carapebus Fm. corresponds to the youngest (potential) source rock reaching a mature state with respect to hydrocarbon generation, if source facies are, indeed, present.

Overall oil and gas windows for kerogen Types I and II – immature <0.5%Ro; *oil window: 0.5–1.3%Ro; **gas window: 1.3–3.0%Ro; ***overmature >3.0%Ro (Tissot & Welte 1978).

2004; Raddadi *et al.* 2008). The origin of the present-day Serra do Mar escarpment is still controversial (Hiruma *et al.* 2010); lateral retreat of the escarpment combined with flexural response can provide important insights regarding the marginal isostatic uplift and the evolution of offshore sedimentary basins in this area (van Balen *et al.* 1995; Hackspacher *et al.* 2004). However, sedimentary supply exceeded the rates of accommodation creation and led to the development of an aggradation–progradation sedimentary architecture (Contreras *et al.* 2010). It is important to note that flexural sediment loading amplified slope gradients and that episodic turbidite deposition persisted from Late Cretaceous times onwards. These gravity mass-flows filled small inter-diapir basins and are partly responsible for syn-sedimentary salt remobilization (Contreras *et al.* 2010).

Since we cannot model for the influence of halokinesis (and/or dissolution of salts), deviations of the *observed tectonic subsidence* from the *modelled subsidence* can probably be attributed to this process: halokinesis is responsible for both the creation and destruction of accommodation space as the salt flows basinwards (thinning near the margin and thickening basinwards as salt-induced structures develop, such as salt windows, welds, pillows, diapirs, etc.: Fig. 1b). In areas where the original salt thickness was greater than presently observed, extra accommodation space may have resulted in the accumulation of a thicker sedimentary sequence. Consequently, the *observed subsidence curves* (after backstripping) would show a greater subsidence during certain periods in the transitional- and post-rift cycles than would be expected tectonically. Similarly, in areas where

Fig. 9. Burial graphs for all shallow-water wells A, B, C and D and deep-water wells E, F and G. For locations see Figure 1. Windows of oil and gas generation for Types I and II kerogen are shown (Tissot & Welte 1978), based on changing maturity values predicted by the best-fit forward model including hydrothermal convection. Note that the rocks deposited between 112 and 90/95 Ma (red curves) contain Type III kerogen for which a different oil/gas window is established (Petersen 2002). Therefore, the oil and gas windows shown here do not apply to the source rocks deposited during this time-frame. Stippled 130 Ma curve corresponds to base Lagoa Feia Fm. (source), but is interpreted from the other modelled curves.

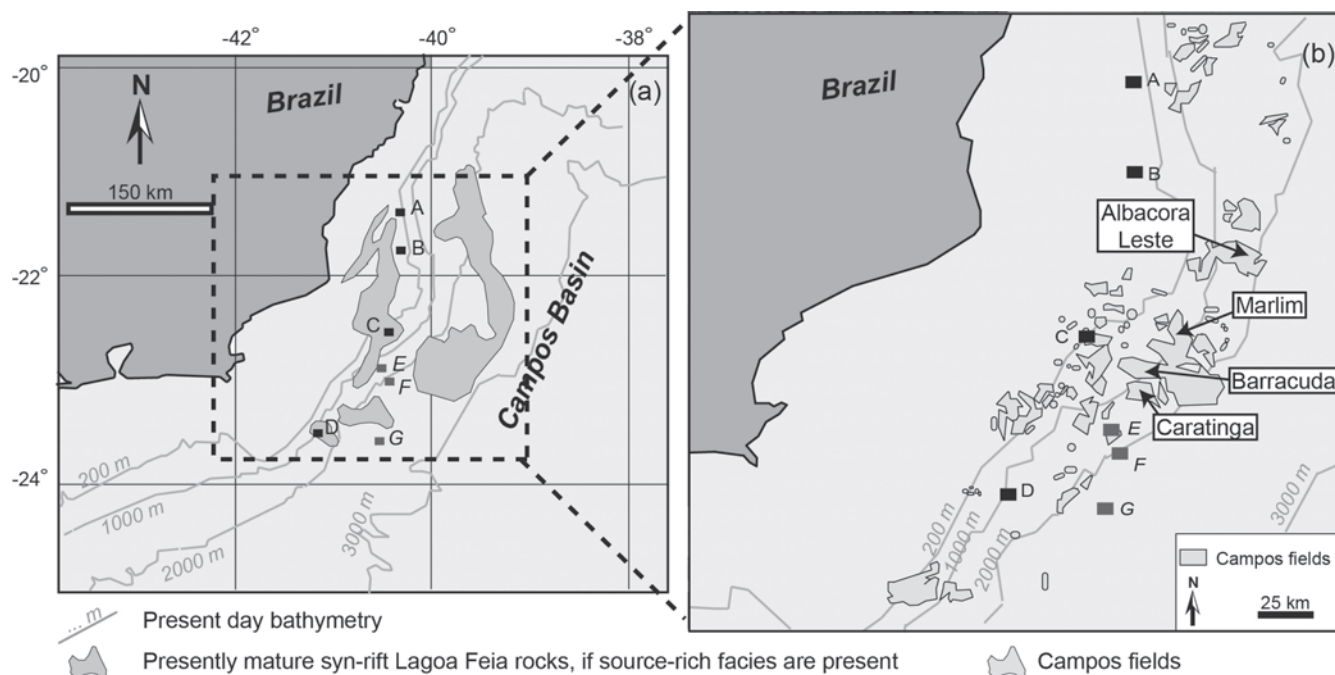


Fig. 10. Campos Basin location maps. (a) Distribution of presently mature syn-rift Lagoa Feia sedimentary rock, if source-rich facies are present, as proposed by Rangel & Martins (1998). (b) Field location. Recently, new oil accumulations have been discovered near several major oil fields, such as Albacora Leste, Marlim, Caratinga and Barracuda.

the original salt sequence was thinner, the decrease in accommodation space due to the formation of salt diapirs and pillows may have resulted in less thick sedimentary sequences: the *observed subsidence* curves would display less subsidence than tectonically expected. Consequently, errors may occur in the modelled lithosphere thickness and heat flow values ($\pm 5\%$ approximately for both), preventing the curves from showing a smooth thickening of the lithosphere and decrease in heat flow. This error range also includes the effects of variations in sedimentary load (and hence subsidence), due to changes in supply. Salt redistribution may also have strongly affected the thermal history of source rocks both beneath and above the salt: due to its high thermal conductivity, salt will delay the maturation of underlying series but, instead, will generate anomalously high geothermal gradients and temperatures above salt pillow and diapirs.

Note also the sudden increase in subsidence rate during the last 28 Ma, particularly in the deep-water wells (Fig. 4e, f). Cloetingh & Kooi (1992) proposed that the Late Neogene accelerations in tectonic subsidence in the deeper parts of rifted basins in the Northern Atlantic could reflect a change in the level of intra-plate stress. Phases of lithospheric compression, due, for example, to Atlantic ridge push (Burov & Cloetingh 2009) during post-rift evolution of rifted basins, can give rise to a substantial deepening of the basin centre, accompanied by uplift at basin flanks. This may also have happened to the Brazilian margin, as seafloor spreading directions and/or rates at the mid-ocean ridge changed. Silver *et al.* (1998) demonstrated that the westward motion of the South American plate accelerated about 30 Ma ago, as the northward absolute motion of the African plate slowed abruptly due to its collision with the Eurasian plate. Both plates are coupled to a general mantle circulation and the spreading velocity on the ridge has remained roughly constant during the last 80 Ma. Therefore, the deceleration of the African plate diverts mantle flow westward, increasing the net basal torque and westward velocity of the South

American plate. Correlations between changes in plate motions and phases of rapid subsidence have also been recognized by Janssen *et al.* (1995) in African basins.

Petroleum system development

Three potential petroleum systems can be distinguished in the Campos Basin: (1) Lagoa Feia–Carapebus PS (!), (2) Macaé–Upper Cretaceous–Carapebus PS (*) and (3) Carapebus–Carapebus PS (?). These petroleum systems are identified at three levels of certainty: (!) known, (*) hypothetical and (?) speculative, indicating the confidence for which a particular pod of active source rock has generated hydrocarbons in an accumulation (Magoon & Dow 1994). Figure 2 illustrates the source–reservoir couples associated with each petroleum system plotted against tectonostratigraphy. Corresponding source-rock properties are given in Table 3.

Source-rock maturation. The overall oil and gas windows are defined as 0.5–1.3%Ro and 1.3–3.0%Ro for kerogen Types I and II (Tissot & Welte 1978). Figure 9 shows the burial curves for each well, combined with the modelled oil and gas windows (for kerogen Types I and II) applying to these wells. The 130 Ma curve does not directly result from modelling, but is an interpretation of the subsidence at the base of the Lagoa Feia Fm. (syn-rift source). Table 4 summarizes when the source rocks of the Lagoa Feia Fm. and Carapebus Fm. entered the oil and/or gas window and shows the state of maturity of each source rock unit at the present day (asterisked).

Rangel & Martins (1998) constructed a map showing where the Lagoa Feia Fm. is mature at the present day, if source-rich facies are, indeed, present (Fig. 10a). The first thing to note is that only wells C and D are located in the proposed area of mature syn-rift source rocks. However, according to our modelling results, the maturity envelope should be expanded to include all wells tested here, excluding wells B and D for the deepest

Table 5. Modelled present-day vitrinite reflectance (%Ro) at base and top Macaé Fm. (112–90 Ma)

Macaé Fm	Vitrinite Reflectance	
	Base (+/- 112 Ma)	Top (+/- 90 Ma)
Wells		
A	0.79	0.65
B	1.23	0.72
C	0.77	0.56
D	0.91	0.82
E	0.74	0.7
F	0.92	0.7
G	0.75	0.55
Oil-window for kerogen type III		Oil-window = 0.85 – 1.8 % Ro
		Immature < 0.85 %Ro

Following Petersen (2002), the oil window is redefined at 0.85–1.8%Ro for kerogen Type III. Note that the Macaé Fm. is only locally mature with respect to oil generation and never reached the gas window.

part of the syn-rift source section (~ overmature: Table 4; Fig. 9b, d). All other wells have a syn-rift source interval located in the oil- and/or gas-generation window.

As for the generative state of the early post-rift Macaé Fm., we refer to Petersen (2002), who demonstrated that the oil window for kerogen Type III should be redefined at vitrinite values of 0.85–1.8%Ro. Although these rocks are generally considered immature, our results show that at least locally (near wells B, D and F) the deepest rock section of the Macaé Fm. seems to have reached the oil window (at present day) (Table 5). No gas will have been generated by the Macaé Fm. source rocks.

The oldest part of the middle/late post-rift Carapebus Fm. seems to have now reached a mature state as well, following the conventional oil window for kerogen Types I and II. The youngest rocks to have reached oil maturity in the last few million years have an age of about 28 Ma and are situated in wells C, D and F (Table 4; Fig. 9c, d, f). However, it is unknown whether source-rich facies are, indeed, present in these relatively young rock sequences. Also note that no mature source rocks that are younger than Turonian in age have yet been drilled in the Campos Basin.

Future prospectivity. Although the Campos Basin has long been Brazil's leading region for oil production, in recent years attention has shifted somewhat towards the Santos Basin in terms of exploration. Presently, Campos produces more than 85% of Brazil's crude oil (Fick 2010).

Recent discoveries of hydrocarbon accumulations in pre-salt layers under certain Petrobras concession areas in the Campos Basin confirm the pre-salt potential of this basin. Since March 2010, pre-salt accumulations have been discovered below the Albacora Leste, Marlim, Caratinga and Barracuda fields (Fig. 10b: Paschoa 2010a, b, c). It is generally agreed that the pre-salt reserves in Campos are certainly not as large as those in the Santos Basin. However, these smaller discoveries are important, since relatively little time and money is needed to get production started: there is already a production infrastructure in place. Furthermore, there remains the possibility of discovering one or two major pre-salt accumulations. The pre-salt accumulation discovered near Barracuda seems to be located in a coquina-reservoir of the Lagoa Feia Fm.. This, in combination with the medium oil found (28° API) (OilVoice 2010), implies that syn-rift lacustrine shales are the source of these hydrocarbons.

To accumulate these oils, the overlying evaporite layer of the transitional cycle needs to be continuous. The coquina reservoir overlies the source shales, allowing for direct migration. Considering the location of this field relatively close to well C and, assuming that the oils originate from the youngest section of source shales, oil generation and accumulation should have started at some time between *c.* 100 Ma and *c.* 58 Ma. According to our modelling, this source section is presently still located in the oil window (Table 4; Fig. 9).

As for post-salt deep-water turbidite reservoirs (Albian–Miocene age), detailed studies have been developed over the last 30 years. Bruhn *et al.* (2009) demonstrated, with seismic amplitude maps of the Marlim Sul and Barracuda fields, the variability and complexity of such turbidite reservoirs. Additionally, these reservoirs may present a large variation in water depth, burial depth, temperature and, therefore, oil quality (Bruhn *et al.* 2009). As for the potential source charging these reservoirs, we can point towards the proven syn-rift lacustrine shales of the Lagoa Feia Fm.. According to our modelling, these shales are mature over a large area, so that generation and migration of hydrocarbons could have taken place at least during some time in basin evolution. However, for these hydrocarbons to reach post-salt reservoirs, migration pathways must exist between the syn-rift and post-rift through the evaporite layer of the transitional cycle. The area we are considering here is characterized by extensional halokinetic movements, in which evaporites are sliding/moving basinwards, creating welds and windows in the salt (Fig. 1b). These salt windows locally allow upward migration of syn-rift-generated hydrocarbons into the post-rift. Further upward migration mainly occurs along salt-induced faults. Furthermore, based on our modelling, the vertical extent of mature sources in the stratigraphy may be viewed more optimistically, which is tentatively supported by these new discoveries in the post-salt section. Our modelling results suggest that the early post-rift Albian Macaé Fm. is locally mature to generate oil (Table 5), while a large section of the Carapebus/Ubatuba Fm. also seems to be located in the oil window (Table 4; Fig. 9). If these late post-rift sedimentary rocks contain sections of organic-rich material (Table 3), oil generation may have occurred. Migration could take place along salt-induced faults as well as by direct contact with the interbedded turbidite reservoirs. Note that no source–oil correlations have been established yet.

CONCLUSION

In this study, we have analysed the tectonic subsidence history of the Campos Basin and developed a tectonic model that explains the observed subsidence history. We applied a combined approach of reverse and forward modelling, in the course of which several model scenarios were tested. The thermal implications of these models were analysed, as well as the consequent source-rock maturation patterns of different potential source-rock intervals.

Recognizing four cycles in basin evolution, we started our subsidence and maturation modelling at the beginning of the syn-rift (145.5 Ma). Three forward models were developed to approach tectonic subsidence as obtained after backstripping.

The first two models (*uniform stretching McKenzie style* and a departure of the *McKenzie model with 4.2 km syn-rift underplating*) could not properly reproduce initial syn-rift tectonic subsidence (as observed after backstripping) or the decrease/stagnation in subsidence during the transitional cycle. Furthermore, they did not provide crustal (β) and mantle (δ) thinning factors, in agreement with both the subsidence record and crustal thickness variations.

The best-fit model includes two underplating phases during the syn-rift and transitional cycles. Modelled thicknesses of the underplated material vary across the basin, as crustal extension factors and initial syn-rift tectonic subsidence vary as well. The greatest underplate thicknesses are modelled during the syn-rift event in the main depocentre. The post-rift cycle is characterized by 'normal' thermal subsidence, which can be subdivided into two phases: a retrogradational sedimentary phase followed by an aggradational-progradational phase, as a result of the uplift of the Serra do Mar mountain range, causing sediment supply to exceed accommodation space created in the Campos Basin from Late Cretaceous times onwards. Therefore, next to thermal cooling, changing volumes of sedimentary load significantly affected post-rift subsidence.

Our best-fit tectonic forward model was tested against measured BHT data. The predicted present-day temperatures within the deep-water wells agree with the measured BHTs. However, in the shallow-water wells (B, C and D) the predicted present-day well temperatures seem systematically higher (20–30°C) than measured. Including the effects of hydrothermal convection within the upper section of the stratigraphy in the shallower parts of the basin results in more effective cooling of the basin sediments: by raising the conductivity of the top part of the stratigraphy (23–0 Ma), the predicted present-day well temperatures are lowered and agree with the measured BHTs.

Unfortunately, we were not able to model for the influence of halokinesis and/or salt dissolution: deviations of the *observed tectonic subsidence* from the *modelled subsidence* (best-fit) can probably be attributed to this process, as halokinesis is capable of both creating and destroying accommodation space. Similarly, salt remobilization may have played an important role in the thermal history of source rocks both below and above the salts, due to its high thermal conductivity.

Our results suggest that the lacustrine shales of the syn-rift Lagoa Feia Fm. are mature to generate oil and/or gas over most of the study area. The marine shales/marls of the early post-rift Macae Fm. are locally mature to generate oil, although gas maturity is not attained. A significant section of the post-rift Carapebus/Ubatuba Fm. may also generate oil, if organic-rich facies intervals are present. Some might view our results with respect to post-salt maturity as rather optimistic. Therefore, it would prove useful to compare these 1D modelling results with 2D simulations, perhaps using commercial software also allowing for lateral transport of salt and overlying sediments through time.

Considering the latest discoveries near established oil fields in the Campos Basin, in both the pre- and post-salt sections, our results support the main expectation that more, as yet undiscovered, accumulations may exist. Generally, the modelled vitrinite reflectance of (potential) source facies is favourable, but the actual presence and distribution of organic-rich facies may provide the greatest risk.

It is not expected that the yet-to-be-discovered accumulations in Campos (in both pre- and post-salt) will be as large as those pre-salt reservoirs in the Santos Basin. However, many more such reservoirs may be discovered, making them important and substantial in total reserves. Furthermore, the production infrastructure already in place will allow these fields to be developed easily.

This work comprises part of S. E. Beglinger's PhD thesis at the VU University of Amsterdam, sponsored by Statoil, and under supervision of Harry Doust and Sierd Cloetingh. The authors would like to thank Statoil for their encouragement and financial support that made this project possible. Furthermore, Statoil – and especially Ian Lunt, Olav Lauvrak and Alexander Schimanski – are thanked for the well data provided and

used in this paper. Special thanks to Ian Lunt, whose comments greatly improved the manuscript, as well as the anonymous reviewers for their keen and very useful remarks and suggestions.

REFERENCES

- Allen, P.A. & Allen, J.R. 2006. *Basin Analysis: Principles and Applications*. Blackwell Science, Oxford.
- An, M. & Assumpção, M. 2006. Crustal and upper mantle structure in the intracratonic Paraná Basin, SE Brazil, from surface wave dispersion using genetic algorithms. *Journal of South American Earth Sciences*, **21**, 173–184.
- Aslanian, D., Moulin, M., Olivet, J.L. et al. 2009. Brazilian and African passive margins of the central segment of the South Atlantic Ocean: kinematic constraints. *Tectonophysics*, **468**, 98–112.
- Bond, G.C. & Kominz, M.A. 1984. Construction of tectonic subsidence curves for the Early Paleozoic miogeocline, southern Canadian Rocky Mountains; implications for subsidence mechanisms, age of breakup and crustal thinning. *Geological Society of America Bulletin*, **95**, 155–173.
- Bott, M.H.P. 1992. Passive margins and their subsidence. *Journal of the Geological Society of London*, **149**, 805–812.
- Boutillier, R.R. & Keen, C.E. 1999. Small-scale convection and divergent plate boundaries. *Journal of Geophysical Research*, **104**, 7389–7403.
- Bruhn, C.H., Pinto, A. & Johann, P.R. 2009. *Main challenges and uncertainties for oil production from turbidite reservoirs in deep water Campos basin, Brazil*. American Association of Petroleum Geologists Search and Discovery Article #10184.
- Burov, E. & Cloetingh, S. 2009. Controls on mantle plumes and lithospheric folding on modes of intraplate continental tectonics: differences and similarities. *Geophysical Journal International*, **178**, 1691–1722.
- Cainelli, C. & Mohriak, W.U. 1999. Some remarks on the evolution of sedimentary basins along the Eastern Brazilian continental margin. *Episodes Journal of International Geoscience*, **22**, 206–216.
- Chang, H.K., Kowsmann, R.O. & Figueiredo, A.M.F. 1988. New concepts of the development of East Brazilian marginal basins. *Episodes Journal of International Geoscience*, **11**, 194–202.
- Chang, H.K., Kowsmann, R.O., Figueiredo, A.M.F. & Bender, A. 1992. Tectonics and stratigraphy of the East Brazil rift system: an overview. *Tectonophysics*, **213**, 97–138.
- Cloetingh, S. & Kooi, H. 1992. Intraplate stresses and dynamical aspects of rifted basins. *Tectonophysics*, **215**, 167–185.
- Cloetingh, S., Beekman, F., Ziegler, P.A., van Wees, J.D. & Sokoutis, D. 2008. Post-rift compressional reactivation potential of passive margins and extensional basins. In: Johnson, H., Doré, A.G., Gatliff, R.W., Holdsworth, R., Lundin, E.R. & Ritchie, J.D. (eds) *The Nature and Origin of Compression in Passive Margins*. Geological Society, London, Special Publications, **306**, 27–70.
- Contreras, J., Zühlke, R., Bowman, S. & Bechstädt, T. 2010. Seismic stratigraphy and subsidence analysis of the Southern Brazilian margin (Campos, Santos and Pelotas basins). *Journal of Marine and Petroleum Geology*, **27**, 1952–1980.
- Coward, M.P., Purdy, E.G., Ries, A.C. & Smith, D.G. 1999. The distribution of petroleum reserves in basins of the South Atlantic margin. In: Cameron, N.R., Bate, R.H. & Clure, V.S. (eds) *The Oil and Gas Habitats of the South Atlantic*. Geological Society, London, Special Publications, **153**, 101–131.
- Cox, K.G. 1980. A model for flood basalt volcanism. *Journal of Petrology*, **21**, 629–650.
- Dupré, S. 2003. *Integrated Study of the South Gabon Margin – Insights on the Rifting Style from Seismic, Well and Gravity Data Analysis and Numerical Modelling*. PhD thesis, VU University Amsterdam.
- Dupré, S., Bertotti, G. & Cloetingh, S. 2007. Tectonic history along the South Gabon basin: anomalous early post-rift subsidence. *Journal of Marine and Petroleum Geology*, **24**, 151–172.
- Estrella, G.O. 1972. Estágio 'rift' nas bacias marginais do leste Brasileiro. *26th Brazilian Geological Congress Proceedings*, **3**, 29–34.
- Fetter, M., De Ros, L.F. & Bruhn, C.H.L. 2009. Petrographic and seismic evidence for the depositional setting of giant turbidite reservoirs and the paleogeographic evolution of Campos basin, offshore Brazil. *Journal of Marine and Petroleum Geology*, **26**, 824–853.
- Fick, J. 2010. *New discoveries sweeten Brazil's Campos basin*. Available online at http://www.rig-zone.com/news/article.asp?a_id=87415.
- Fjeldskaar, W., Johansen, H., Dodd, T.A. & Thompson, M. 2003. *Temperature and maturity effects of magmatic underplating in the Gjallar Ridge, Norwegian Sea, multidimensional basin modelling*. American

- Association of Petroleum Geologists (AAPG/Datapages), Tulsa, OK, 71–85.
- Foucher, J.-P., Le Pichon, X. & Sibuet, J.-C. 1982. The ocean–continent transition in the uniform lithospheric stretching model: role of partial melting in the mantle. *Philosophical Transactions of the Royal Society of London. Series A, Mathematical and Physical Sciences*, **305**, 27–43.
- Furlong, K.P. & Fountain, D.M. 1986. Lithospheric evolution with underplating: thermal considerations and seismic-petrologic consequences. *Journal of Geophysical Research*, **91**, 8285–8294.
- Gallagher, K. & Hawkesworth, C. 1994. Mantle plumes, continental magmatism and asymmetry in the South Atlantic. *Earth and Planetary Science Letters*, **123**, 105–117.
- Gernigon, L., Ringenback, J.C., Planke, S. & Le Gall, B. 2004. Deep structures and breakup along volcanic rifted margins: insights from integrated studies along the Outer Vøring basin (Norway). *Journal of Marine and Petroleum Geology*, **21**, 363–372.
- Guardado, L.R., Spadini, A.R., Brandao, J.S.L. & Mello, M.R. 2000. Petroleum system of the Campos basin, Brazil. In: Mello, M.R. & Katz, B.J. (eds) *Petroleum Systems of South Atlantic Margins*. American Association of Petroleum Geologists Memoir, **73**, 317–324.
- Hackspacher, P.C., Ribeiro, L.F.B., Ribeiro, M.C.S., Fetter, A.H., Hadler Neto, J.C., Tello, C.E.S. & Dantas, E.L. 2004. Consolidation and breakup of the South American Platform in Southeastern Brazil: tectonothermal and denudation histories. *Gondwana Research*, **7**, 91–101.
- Hawkesworth, C.J., Gallagher, K., Kelley, S., Mantovani, M., Peate, D.W., Regelous, M. & Rogers, N.W. 1992. Parana magmatism and the opening of the South Atlantic. In: Storey, B.C., Alabaster, T. & Pankhurst, R.J. (eds) *Magmatism and the Causes of Continental Break-up*. Geological Society, London, Special Publications, **68**, 221–240.
- Hirsch, K.K., Scheck-Wenderoth, M., van Wees, J.D., Kuhlman, G. & Paton, D.A. 2010. Tectonic subsidence history and thermal evolution of the Orange basin. *Journal of Marine and Petroleum Geology*, **27**, 565–584.
- Hiruma, S.T., Riccomini, C., Modenesi-Gauttieri, M.C., Hackspacher, P.C., Hadler Neto, J.C. & Franco-Magalhães, A.O.B. 2010. Denudation history of the Bocaina Plateau, Serra do Mar, Southeastern Brazil: relationships to Gondwana breakup and passive margin development. *Gondwana Research*, **18**, 674–687.
- Janssen, M.E., Stephenson, R.A. & Cloetingh, S. 1995. Temporal and spatial correlations between changes in plate motions and the evolution of rifted basins in Africa. *Geological Society of America Bulletin*, **107**, 1317–1332.
- Karner, G.D. 2000. Rifts of the Campos and Santos basins, Southeastern Brazil: distribution and timing. In: Mello, M.R. & Katz, B.J. (eds) *Petroleum Systems of South Atlantic Margins*. American Association of Petroleum Geologists Memoir, **73**, 301–315.
- Karner, G.D. & Gambôa, L.A.P. 2007. Timing and origin of the South Atlantic pre-salt sag basins their capping evaporites. In: Schreiber, B.C., Lugli, S. & Babel, M. (eds) *Evaporites through Space and Time*. Geological Society, London, Special Publications, **285**, 15–35.
- Khain, V.E. & Polyakova, I.D. 2004. Oil and gas potential of deep- and ultradeep-water zones of continental margins. *Lithology and Mineral Resources*, **39**, 530–540.
- Kuszniir, N.J., Roberts, A.M. & Morley, C.K. 1995. Forward and reverse modelling of rift basin formation. In: Lambiase, J.J. (ed.) *Hydrocarbon Habitat in Rift Basins*. Geological Society, London, Special Publications, **80**, 33–56.
- Kuszniir, N.J., Hunsdale, R. & Roberts, A.M. (iSIMMTeam) 2005. Timing and magnitude of depth-dependent lithosphere stretching on the Southern Lofoten and Northern Vøring continental margins offshore Mid-Norway: implications for subsidence and hydrocarbon maturation at volcanic rifted margins. In: Doré, A.G.V. (ed.) *Petroleum Geology: North-West Europe and Global Perspectives – Proceedings of the 6th Petroleum Geology Conference*. Geological Society, London, 767–783.
- Lobo, A.P. & Ferradaes, J.O. 1983. *Reconhecimento preliminar do talude e sopé continentais da bacia de Campos*. Petrobrás Internal Report, Depex Rio de Janeiro.
- Luijendijk, E., ter Voorde, M., van Balen, R.T., Verweij, H. & Simmeling, E. 2011. Thermal state of the Roer Valley Graben, part of the European Cenozoic rift system. *Basin Research*, **1**, 65–82.
- Magoon, L.B. & Dow, W.G. 1994. The petroleum system. In: Magoon, L.B. & Dow, W.G. (eds) *The Petroleum System – from Source to Trap*. American Association of Petroleum Geologists Memoir, **60**, 3–24.
- McKenzie, D.P. 1978. Some remarks on the development of sedimentary basins. *Earth and Planetary Science Letters*, **40**, 25–32.
- Meisling, K.E., Cobbold, P.R. & Mount, V.S. 2001. Segmentation of an obliquely rifted margin, Campos and Santos basins, Southeastern Brazil. *American Association of Petroleum Geologists Bulletin*, **85**, 1903–1924.
- Mello, M.R., Mohriak, W.U., Koutsoukos, E.A.M. & Bacocoli, G. 1994. Selected petroleum systems in Brazil. In: Magoon, L.B. & Dow, W.G. (eds) *The Petroleum System – from Source to Trap*. American Association of Petroleum Geologists Memoir, **60**, 499–512.
- Milner, S.C., Duncan, A.R., Whittingham, A.M. & Ewart, A. 1995. Trans-Atlantic correlation of eruptive sequences and individual silicic volcanic units within the Paraná-Etendeka igneous province. *Journal of Volcanology and Geothermal Research*, **69**, 137–157.
- Mizusaki, A.M.P., Petrini, R., Bellieni, G., Cominchiaramonti, P., Dias, J., Demin, A. & Piccirillo, E.M. 1992. Basalt magmatism along the passive continental margin of SE Brazil (Campos Basin). *Contributions to Mineralogy and Petrology*, **111**, 143–160.
- Modica, C.J. & Brush, E.R. 2004. Post-rift sequence stratigraphy, paleogeography and fill history of the deep-water Santos basin, offshore Southeast Brazil. *American Association of Petroleum Geologists Bulletin*, **88**, 923–945.
- Mohriak, W.U. & Dewey, J.F. 1987. Deep seismic reflectors in the Campos basin, offshore Brazil. *Geophysical Journal of the Royal Astronomical Society*, **89**, 133–140.
- Mohriak, W.U., Karner, G.D. & Dewey, J.F. 1987. Subsidence history and tectonic evolution of the Campos basin, offshore Brazil (abstract). *American Association of Petroleum Geologists*, **71**, 594.
- Mohriak, W.U., Mello, M.R., Dewey, J.F. & Maxwell, J.R. 1990a. Petroleum geology of the Campos basin, offshore Brazil. In: Brooks, J. (ed.) *Classic Petroleum Provinces*. Geological Society, London, Special Publications, **50**, 119–141.
- Mohriak, W.U., Hobbs, R. & Dewey, J.F. 1990b. Basin-forming processes and the deep structure of the Campos basin, offshore Brazil. *Journal of Marine and Petroleum Geology*, **7**, 94–122.
- Moulin, M., Aslanian, D., Olivet, J.-L. *et al.* 2005. Geological constraints on the evolution of the Angolan margin based on reflection and refraction seismic data (Zaiango project). *Geophysical Journal International*, **162**, 793–810.
- OilVoice. 2010. *Petrobras announces oil discovery in deep Campos basin waters*. Available online at http://www.oilvoice.com/n/Petrobras_Announces_Oil_Discovery_in_Deep_Campos_Basin_Waters/af6138cb0.aspx.
- Ojeda, H.A.O. 1982. Structural framework, stratigraphy and evolution of Brazilian marginal basins. *American Association of Petroleum Geologists Bulletin*, **66**, 732–749.
- Paschoa, C. 2010a. *New pre-salt discovery at the Marlim field*. Available online at <http://news.seadiscovery.com/post/2010/06/04/presalt-discovery-marlim-field.aspx>.
- Paschoa, C. 2010b. *New discovery confirms the Campos basin pre-salt potential*. Available online at <http://news.seadiscovery.com/post/2010/06/23/discovery-confirms-presalt-potential.aspx>.
- Paschoa, C. 2010c. *New discovery confirms the Campos basin pre-salt potential*. Available online at <http://www.maritimeprofessional.com/Blogs/Brazilian-subsea-news/June-2010-New-Discovery-Confirms-the-Campos-Basin-Pre-Salt-P.aspx>.
- Peate, D.W. 1997. The Paraná–Etendeka province. In: Mahoney, J.J. & Coffin, M.F. (eds) *Large Igneous Provinces: Continental, Oceanic and Planetary Flood Volcanism*. *Geophysical Monographs*, **100**, 217–245.
- Pedersen, T. & Ro, H.E. 1992. Finite duration extension and decompression melting. *Earth and Planetary Science Letters*, **113**, 15–22.
- Petersen, H.I. 2002. A re-consideration of the ‘oil-window’ for humic coal and kerogen type III source rocks. *Journal of Petroleum Geology*, **25**, 407–432.
- Raddadi, M.C., Hoult, R.J. & Markwich, P.J. 2008. *The Late Cretaceous uplift history of the South Atlantic continental margins: examples from the Santos and Campos basins of Southeast Brazil*. American Association of Petroleum Geologists Search and Discovery Article #90078.
- Rangel, H.D. & Martins, C.C. 1998. Main exploratory compartments, Campos basin, Chapter 2: Geologic Scenario in the Brazilian Sedimentary Basins. In: *Searching for Oil and Gas in the Land of Giants: Search*. Schlumberger, Rio de Janeiro, 32–40.
- Ranalli, G. & Rybach, L. 2005. Heat flow, heat transfer and lithosphere rheology in geothermal areas: features and examples. *Journal of Volcanology and Geothermal Research*, **148**, 3–19.
- Renne, P.R., Ernesto, M., Pacca, I.G. *et al.* 1992. The age of Paraná flood volcanism, rifting of Gondwanaland, and the Jurassic–Cretaceous boundary. *Science*, **258**, 975–979.
- Renne, P.R., Glen, J.M., Milner, S.C. & Duncan, A.R. 1996. Age of Etendeka flood volcanism and associated intrusions in southwestern Africa. *Geology*, **24**, 659–662.
- Renner, J.L., White, D.E. & Williams, D.L. 1975. Hydrothermal convection systems. In: White, D.E. & Williams, D.L. (eds) *Assessment of*

- Geothermal Resources of the United States – 1975*. U.S. Geological Survey Circular, 5–57.
- Roberts, A.M., Kusznir, N.J., Yielding, G. & Styles, P. 1998. 2D flexural backstripping of extensional basins: the need for a sideways glance. *Petroleum Geoscience*, **4**, 327–338.
- Rowley, D.B. & Sahagian, D. 1986. Depth-dependent stretching: a different approach. *Geology*, **14**, 32–35.
- Royden, L. & Keen, C.E. 1980. Rifting process and thermal evolution of the continental margin of Eastern Canada determined from subsidence curves. *Earth and Planetary Science Letters*, **51**, 343–361.
- Sclater, J.G. & Christie, P.A.F. 1980. Continental stretching: an explanation of the Post-Mid-Cretaceous subsidence of the Central North Sea basin. *Journal of Geophysical Research*, **85**, 3711–3739.
- Scotchman, I.C., Gilchrist, G., Kusznir, N.J., Roberts, A.M. & Fletcher, R. 2010. The breakup of the South Atlantic Ocean: formation of failed spreading axes and blocks of thinned continental crust in the Santos basin, Brazil and its consequences for petroleum system development. In: Vining, B.A. & Pickering, S.C. (eds) *Petroleum Geology: From Mature Basins to New Frontiers – Proceedings of the 7th Petroleum Geology Conferences*. Geological Society, London, 855–866.
- Silver, P.G., Russo, R.M. & Lithgow-Bertelloni, C. 1998. Coupling of South American and African plate motion and deformation. *Science*, **279**, 60–63.
- Skogseid, J., Planke, S., Faleide, J.L., Pedersen, T., Eldholm, O. & Neverdal, F. 2000. NE Atlantic continental rifting and volcanic margin formation. In: Nøttvedt, A. (ed.) *Dynamics of the Norwegian Margin*. Geological Society, London, Special Publications, **167**, 295–326.
- Spinelli, G.A. & Fisher, A.T. 2004. Hydrothermal circulation within topographically rough basaltic basement on the Juan de Fuca Ridge flank. *Geochemistry, Geophysics, Geosystems*, **5**, 1–19.
- Sweeney, J.J. & Burnham, A.K. 1990. Evaluation of a simple model for vitrinite reflectance based on chemical kinetics. *American Association of Petroleum Geologists Bulletin*, **74**, 1559–1570.
- Thompson, R.N., Gibson, S.A., Mitchell, J.G., Dickin, A.P., Leonardos, O.H., Brod, J.A. & Greenwood, J.C. 1998. Migrating Cretaceous–Eocene magmatism in the Serra do Mar alkaline province, SE Brazil: melts from the deflected Trindade mantle plume? *Journal of Petrology*, **39**, 1493–1526.
- Tissot, B.P. & Welte, D.H. 1978. *Petroleum Formation and Occurrence*, 2nd edn. Springer-Verlag, New York.
- Van Balen, R.T., van der Beek, P.A. & Cloetingh, S. 1995. The effect of rift shoulder erosion on stratal patterns at passive margins: implications for sequence stratigraphy. *Earth and Planetary Science Letters*, **134**, 527–544.
- Van Wees, J.D. & Beekman, F. 2000. Lithosphere rheology during intraplate basin extension and inversion: inferences from automated modelling of four basins in Western Europe. *Tectonophysics*, **320**, 219–242.
- Van Wees, J.D. & Stephenson, R.A. 1995. Quantitative modelling of basin and rheological evolution of the Iberian basin (Central Spain): implications for lithospheric dynamics and intraplate extension and inversion. *Tectonophysics*, **252**, 163–178.
- Van Wees, J.D., van Bergen, F., David, P., Nepveu, M., Beekman, F., Cloetingh, S. & Bonté, D. 2009. Probabilistic tectonic heat flow modelling for basin maturation: assessment method and applications. *Journal of Marine and Petroleum Geology*, **26**, 536–551.
- Van Wijk, J., Huismans, R.S., ter Voorde, M. & Cloetingh, S. 2001. Melt generation at volcanic continental margins: no need for a mantle plume? *Geophysical Research Letters*, **28**, 3995–3998.
- Vilà, M., Fernández, M. & Jiménez-Munt, I. 2010. Radiogenic heat production variability of some common lithological groups and its significance to lithospheric thermal modelling. *Tectonophysics*, **490**, 152–164.
- Watts, A.B. & Fairhead, J.D. 1999. A process-oriented approach to modelling the gravity signature of continental margins. *The Leading Edge*, **18**, 258–263.
- Wilson, M. 1992. Magmatism and continental rifting during the opening of the South Atlantic: a consequence of Lower Cretaceous superplume activity? In: Storey, B.C., Alabaster, T. & Pankhurst, R.J. (eds) *Magmatism and the Causes of Continental Break-up*. Geological Society, London, Special Publications, **68**, 241–255.
- Ziegler, P.A. 1992. Geodynamics of rifting and implications for hydrocarbon habitat. *Tectonophysics*, **215**, 221–253.

Received 15 October 2010; revised typescript accepted 24 February 2012.